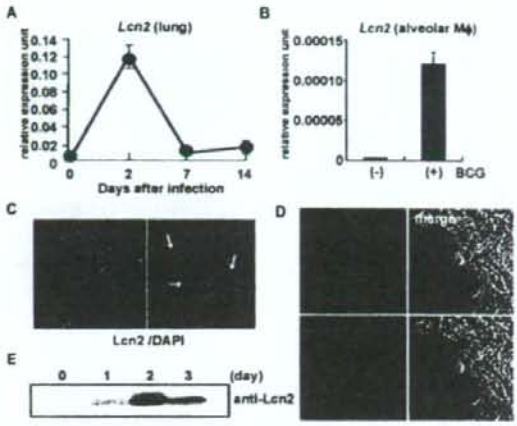

FIGURE 1. Lcn2 expression in the lungs of BCG-infected mice. *A*, Wild-type C57BL/6 mice were intratracheally infected with 2.5×10^6 CFU of BCG. Total RNA was extracted from the lungs after the indicated periods. Lcn2 mRNA expression was analyzed by real-time quantitative PCR. Data are shown as the relative mRNA levels normalized by the corresponding 18S rRNA level. Data are presented as means ± SD, and are representative of two independent experiments. *B*, Alveolar macrophages were isolated from uninfected wild-type mice, cultured with or without BCG for 48 h, and then analyzed for their Lcn2 mRNA expression by real-time quantitative PCR. *C* and *D*, At 2 days after intratracheal infection with BCG, lung tissue sections were stained with anti-Lcn2 Ab (red), DAPI (blue), and anti-SP-C Ab (green), and visualized by fluorescence microscopy. *E*, Wild-type mice were intratracheally infected with 2.5×10^6 CFU of BCG. At the indicated time points after the infection, 500 μl of PBS was intratracheally injected and then recovered. The recovered BALF samples were subjected to Western blot analysis with anti-Lcn2 Ab.

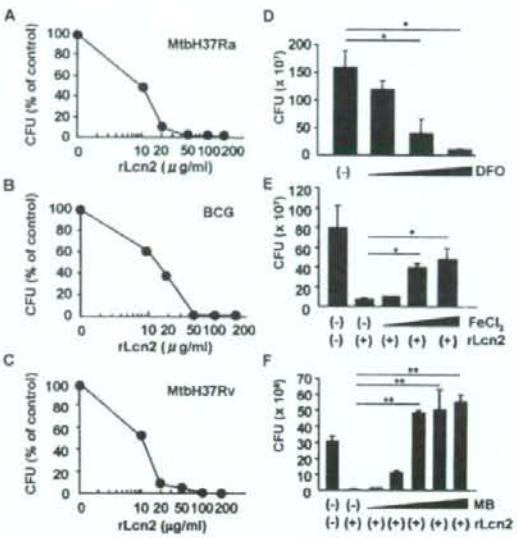

FIGURE 2. Inhibition of in vitro mycobacterial growth by Lcn2. *A–C*, *M. tuberculosis* H37Ra (*A*), BCG (*B*), or *M. tuberculosis* H37Rv (*C*) (1×10^5 CFU each) was incubated with the indicated concentrations of rLcn2 in 7H9 ADC medium for 20 days and then plated on 7H10-OADC agar. The CFU numbers were counted. *D*, BCG was incubated with increasing concentrations of DFO (1 μM, 100 μM and 1 mM) for 20 days and then plated on 7H10-OADC agar. The CFU numbers were counted. *E* and *F*, BCG was incubated in the presence of rLcn2 (50 μg/ml) as well as increasing concentrations of $FeCl_3$ (*E*: 5 nM, 500 nM, 50 μM, and 5 mM) or MB (*F*: 1 pg/ml, 10 pg/ml, 1 ng/ml, 100 ng/ml, and 10 μg/ml) (*F*) for 20 days, and then plated on 7H10-OADC agar. All data are presented as means ± SD. * and ** indicate a significant difference among groups. ANOVA, posthoc Scheffe, *, $p < 0.05$; **, $p < 0.005$.

after infection; BCG infection led to a marked increase in the expression of Lcn2 mRNA. We also analyzed the lungs by immunohistochemistry using an anti BCG-infected mice, several Lcn2-positive cells were observed. These cells mainly faced the alveolar surface and projected into the alveolar space, representing the typical morphology of type II alveolar epithelial cells. Costaining with an Ab to pro-SP-C, which is produced by type II alveolar epithelial cells, revealed that both Lcn2 and SP-C were produced by the same cells (Fig. 1*D*). These findings indicate that not only alveolar macrophages but also type II alveolar epithelial cells produce Lcn2 during respiratory mycobacterial infection. Type II alveolar epithelial cells are known to secrete several mediators into the alveolar space. Therefore, we analyzed whether Lcn2 is secreted into the alveolar space during intratracheal BCG infection. BALF was collected from uninfected and BCG-infected mice and analyzed for Lcn2 protein expression by Western blotting (Fig. 1*E*). Lcn2 was not detected in BALF from uninfected mice. At 2 days after BCG infection, Lcn2 expression was abundantly detected in BALF from the infected mice, indicating that Lcn2 was secreted into the alveolar space during the early phase of mycobacterial infection.

Lcn2-mediated inhibition of mycobacterial growth

We produced rLcn2 and analyzed its effect on in vitro mycobacterial growth. Addition of rLcn2 dose-dependently inhibited the growth of avirulent strains of mycobacteria such as BCG and *M. tuberculosis* H37Ra (Fig. 2, *A* and *B*). rLcn2 also inhibited the growth of virulent *M. tuberculosis* H37Rv in a dose-dependent manner (Fig. 2*C*). Thus, Lcn2 has the ability to inhibit the growth of several mycobacterial strains.

We investigated whether Lcn2 inhibits mycobacterial growth by interfering with iron acquisition, similar to the case for inhibition of *E. coli* growth (16). First, we added DFO, an iron chelator, into in vitro BCG cultures (Fig. 2*D*). DFO reduced BCG growth in a dose-dependent manner, indicating that BCG requires iron for growth. Next, we added ferric iron into BCG cultures (Fig. 2*E*). Addition of ferric iron rescued Lcn2-mediated inhibition of BCG growth in a dose-dependent manner, indicating that Lcn2 inhibits use of iron from the culture medium. Addition of exogenous mycobactin (MB) also abolished Lcn2-mediated inhibition of BCG growth (Fig. 2*F*). These findings indicate that Lcn2 inhibits mycobacterial growth by sequestering iron.

In vivo anti-mycobacterial activity of lipocalin 2

We next addressed the in vivo role of Lcn2 in *M. tuberculosis* infection using $Lcn2^{-/-}$ mice. Wild-type and $Lcn2^{-/-}$ mice were intratracheally infected with *M. tuberculosis* H37Rv and monitored for their survival (Fig. 3*A*). $Lcn2^{-/-}$ mice were highly sensitive to intratracheal infection with *M. tuberculosis* and many of the infected mice died. We also counted the CFU numbers in the lungs and livers after 6 wk of infection (Fig. 3*B*). The CFU titer of *M. tuberculosis* was higher in $Lcn2^{-/-}$ mice than that in wild-type mice. Histopathological analysis of the lungs of the infected mice at 20 days after infection revealed that the number and size of the granulomatous lesions were increased in $Lcn2^{-/-}$ mice (Fig. 3*C*), indicating that the inflammatory response in $Lcn2^{-/-}$ mice was enhanced, possibly due to progression of the *M. tuberculosis* infection. These findings demonstrate that Lcn2 plays an important role in host resistance to *M. tuberculosis* infection in vivo.

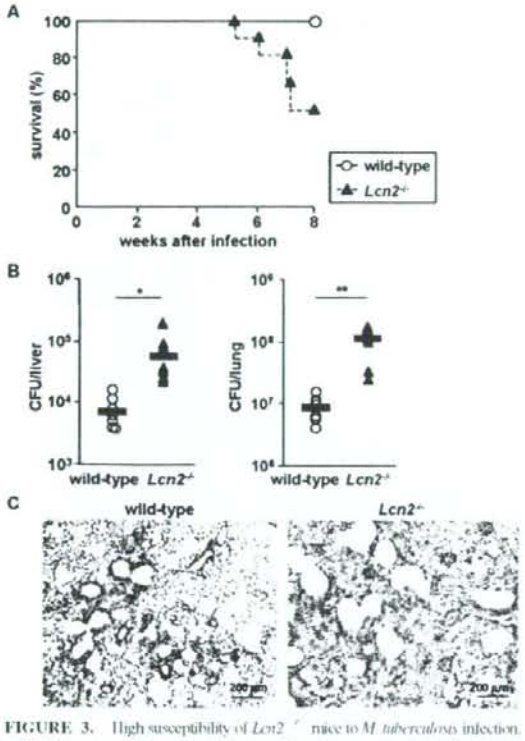

FIGURE 3. High susceptibility of *Lcn2*$^{-/-}$ mice to *M. tuberculosis* infection. *A*, Wild type (*n* = 11) and *Lcn2*$^{-/-}$ (*n* = 12) mice were intratracheally infected with *M. tuberculosis* H37Rv (1×10^6 CFU) and their survival was monitored for 8 wk. *B*, Wild type (*n* = 7) and *Lcn2*$^{-/-}$ (*n* = 7) mice were intratracheally infected with *M. tuberculosis* H37Rv (1×10^6 CFU). At 6 wk after infection, homogenates of the lungs and livers were plated on 7H10 OADC agar and the CFU titers were counted. Symbols represent individual mice, and bars represent the mean CFU numbers. *, $p < 0.05$; **, $p < 0.005$. Data are representative of two independent experiments. *C*, H&E staining of representative lung tissues from wild-type and *Lcn2*$^{-/-}$ mice at 20 days after intratracheal infection with *M. tuberculosis*.

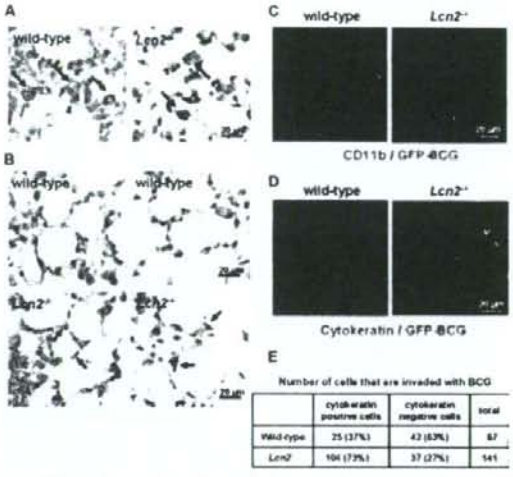

FIGURE 4. Increased numbers of *M. tuberculosis* in *Lcn2*$^{-/-}$ alveolar epithelial cells. *A* and *B*, Wild type and *Lcn2*$^{-/-}$ mice were intratracheally infected with *M. tuberculosis* H37Ra. At 5 days after infection, the lungs were fixed in paraffin, sectioned, and stained with the Ziehl-Neelsen method. Arrows indicate red stained *M. tuberculosis*. *C–E*, At 5 days after intratracheal infection with GFP expressing BCG (green), lung tissue sections were stained with anti CD11b Ab (*C*, red) or anti-pan-cytokeratin Ab (*D*, red), and visualized by fluorescence microscopy. The number of cells containing BCG was counted in a total of ten areas of pictures that visualized different fields (*E*).

Increased numbers of mycobacteria in Lcn2-deficient alveolar epithelial cells

We next analyzed the localization of *M. tuberculosis* in the lungs at 5 days after intratracheal infection by staining acid-fast bacilli using the Ziehl-Neelsen method. In wild-type and *Lcn2*$^{-/-}$ mice, similar densities of *M. tuberculosis* were observed in granulomatous lesions, although the number and size of the granulomatous lesions were increased in *Lcn2*$^{-/-}$ mice (data not shown). In addition, *M. tuberculosis* exhibited similar staining of cells with a macrophage-like morphology in wild-type and *Lcn2*$^{-/-}$ mice (Fig. 4*A*). Strikingly, some of the alveolar epithelial cell layers in *Lcn2*$^{-/-}$ mice contained *M. tuberculosis* (Fig. 4*B*). In sharp contrast, *M. tuberculosis* was scarcely detected within the epithelial cell layers of wild-type mice. To corroborate these findings, we subjected the lungs of mice intratracheally infected with GFP-expressing BCG to immunohistochemical analyses. In both wild-type and *Lcn2*$^{-/-}$ mice, CD11b-positive cells contained GFP-expressing BCG. However, in the lungs of *Lcn2*$^{-/-}$ mice, GFP-expressing BCG was frequently observed in cells that did not express CD11b, in contrast to the low frequency observed in the lungs of wild-type mice (Fig. 4*C*). Visualization of epithelial cells using an anti-cytokeratin Ab indicated that increased numbers of alveolar epithelial cells in *Lcn2*$^{-/-}$ mice contained GFP-expressing BCG compared with those in wild-type mice (Fig. 4, *D* and *E*). Thus, in the absence of Lcn2, invasion and replication of mycobacteria in alveolar epithelial cells were increased.

Therefore, we assessed the sensitivities of alveolar macrophages and alveolar epithelial cells to in vitro infection with BCG. First, alveolar macrophages were isolated from wild-type and *Lcn2*$^{-/-}$ mice, and infected with BCG (Fig. 5*A*). The CFU titers of BCG in macrophages at 4 and 7 days after infection were comparable between wild-type and *Lcn2*$^{-/-}$ cells. Thus, the absence of Lcn2 did not affect the anti-mycobacterial activity in alveolar macrophages. Next, we established AECs from wild-type and *Lcn2*$^{-/-}$ mice. Because AECs are difficult to culture in vitro, we took advantage of transgenic mice harboring a temperature-sensitive mutation of the SV40 large tumor Ag gene under the control of an IFN-γ-inducible H-2K^b promoter element (30–32). Using these mice, we successfully established wild-type and *Lcn2*$^{-/-}$ AECs, both of which were stained with anti-SP-C Ab (data not shown). AECs from wild-type mice expressed Lcn2 mRNA and secreted Lcn2 protein into the culture medium when infected with BCG (data not shown). Thus, these AECs showed the characteristics of type II alveolar epithelial cells. AECs were infected with BCG, and the CFU titers within the cells were counted at 1, 2, 3, and 4 days after infection (Fig. 5*B*). At 3 and 4 days after infection, the CFU titers in *Lcn2*$^{-/-}$ cells were increased compared with those in wild-type cells. Addition of exogenous Lcn2 reduced the CFU numbers in *Lcn2*$^{-/-}$ cells (Fig. 5*C*). Taken together, these findings indicate that the high susceptibility of *Lcn2*$^{-/-}$ mice to *M. tuberculosis* infection is attributable to impaired clearance of mycobacteria from alveolar epithelial cells, rather than alveolar macrophages, in the absence of Lcn2.

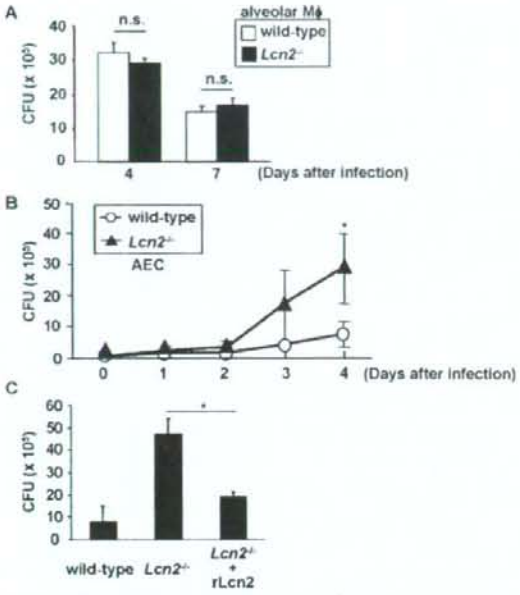

FIGURE 5. Increased BCG growth in *Lcn2* $^{-/-}$ alveolar epithelial cells. *A*, Alveolar macrophages were collected from uninfected wild-type and *Lcn2* $^{-/-}$ mice and cultured with BCG for the indicated periods. To eliminate external BCG, the cells were cultured with streptomycin for 1 h, washed three times, and harvested. Lysates of the cells were plated on 7H10-OADC agar, and the CFU numbers were counted. Representative data of two independent experiments are shown. n.s., not significant. *B*, Wild-type and *Lcn2* $^{-/-}$ AECs were cultured with BCG for the indicated periods. After removal of extracellular BCG, lysates the cells were plated on 7H10-OADC agar, and the CFU numbers were counted. Data are presented as means ± SD of triplicate determinations and are representative of three independent experiments. *, $p < 0.05$. Similar results were obtained when other AECs from wild-type and *Lcn2* $^{-/-}$ mice were used. *C*, Wild-type and *Lcn2* $^{-/-}$ AECs were cultured with BCG. At 2 days after infection, rLcn2 (final concentration 30 μg/ml) was added to the *Lcn2* $^{-/-}$ AEC. After an additional 2 days of culture, the cells were incubated with streptomycin for 1 h, washed three times, and harvested. Lysates of the cells were plated on 7H10-OADC agar, and the CFU numbers were counted. Representative data of three independent experiments are shown. Data are presented as means ± SD of triplicate determinations. *, $p < 0.05$.

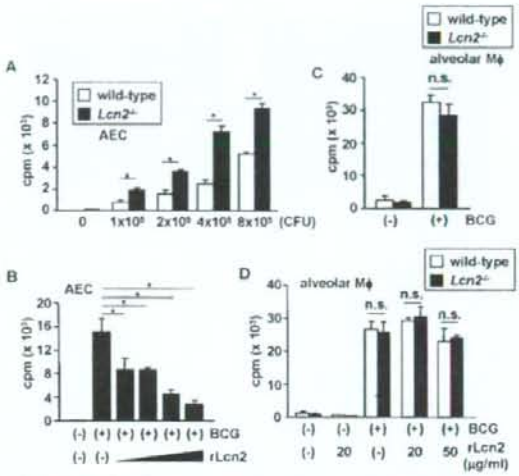

FIGURE 6. Lcn2-mediated inhibition of intracellular BCG growth. *A*, Wild-type and *Lcn2* $^{-/-}$ AECs were seeded onto 96-well plates and infected with the indicated CFUs of BCG for 6 h. The cells were then extensively washed to remove extracellular BCG and cultured in the presence of [^{3}H]uracil for 48 h. The incorporation of [^{3}H]uracil was measured. Data are presented as means ± SD of triplicate samples. Representative data of three independent experiments are shown. *, $p < 0.005$. *B*, *Lcn2* $^{-/-}$ AECs were seeded onto 96-well plates, and infected with BCG (2×10^5 CFU) for 6 h. After vigorous washing, the cells were cultured with increasing concentrations of rLcn2 (20, 30, 40, and 50 μg/ml) and [^{3}H]uracil for 48 h, before being measured for their [^{3}H]uracil incorporation. Data are presented as means ± SD of triplicate samples, and are representative of two independent experiments. + indicate a significant difference among groups, ANOVA, posthoc Scheffe, *, $p < 0.001$. *C*, Alveolar macrophages were collected from uninfected wild-type and *Lcn2* $^{-/-}$ mice, and cultured with BCG for 6 h. After vigorous washing, the cells were cultured in the presence of [^{3}H]uracil for 48 h, before being measured for their [^{3}H]uracil incorporation. Data are presented as the mean ± SD of triplicate samples. n.s., not significant. *D*, Alveolar macrophages from wild-type and *Lcn2* $^{-/-}$ mice were infected with BCG for 6 h. After vigorous washing, the cells were cultured in the presence of the indicated concentration of rLcn2 and [^{3}H]uracil for 48 h. Then, the [^{3}H]uracil incorporation was counted. Data are presented as means ± SD of triplicate samples. n.s., not significant.

Inhibition of intracellular mycobacterial growth by Lcn2

Mycobacteria are intracellular bacteria that replicate within cells. In the experiments performed so far, it is possible that extracellular growth was monitored as well as intracellular growth under the in vitro conditions. Therefore, to assess the intracellular growth of mycobacteria more precisely, we used [^{3}H]uracil, which is preferentially incorporated into mycobacterial nucleic acids (33). AECs derived from wild-type and *Lcn2* $^{-/-}$ mice were infected with several CFUs of BCG for 6 h, extensively washed with culture medium containing streptomycin to exclude extracellular BCG, and then cultured for 2 days in the presence of [^{3}H]uracil (Fig. 6*A*). Under these conditions, [^{3}H]uracil incorporation was below 1×10^2 cpm in wells containing uninfected AECs or wells placed in contact with BCG and then extensively washed. After infection with each CFU, [^{3}H]uracil incorporation was increased in *Lcn2* $^{-/-}$ cells compared with wild-type cells. In BCG-infected *Lcn2* $^{-/-}$ cells, addition of exogenous rLcn2 reduced the uptake of [^{3}H]uracil by intracellular BCG (Fig. 6*B*). In alveolar macrophages, the [^{3}H]uracil incorporation by intracellular BCG was comparable between wild-type and *Lcn2* $^{-/-}$ cells (Fig. 6*C*). Addition of rLcn2 did not effectively reduce the uptake of [^{3}H]uracil by intracellular BCG in alveolar macrophages from both wild-type and *Lcn2* $^{-/-}$ mice (Fig. 6*D*). These findings indicate that extracellular Lcn2 limits intracellular growth of BCG in AECs, but not in alveolar macrophages.

Because extracellular Lcn2 modulated intracellular mycobacterial growth in the AECs, we analyzed whether extracellular Lcn2 was incorporated into the AECs as described in several previous reports (18, 19). AECs were infected with GFP-expressing BCG and then treated with fluorescein-labeled rLcn2 (Fig. 7*A*). Lcn2 was detected within the AECs, and colocalized with dextran that was taken up into the cells by endocytosis. Furthermore, many BCG were colocalized with rLcn2, indicating that endocytosed Lcn2 was in close proximity to intracellular BCG. In contrast, although Lcn2 was incorporated into alveolar macrophages, the incorporated Lcn2 was not colocalized with BCG in alveolar macrophages (Fig. 7*B*), indicating that BCG and rLcn2 were localized in distinct cellular compartments within macrophages. We blocked

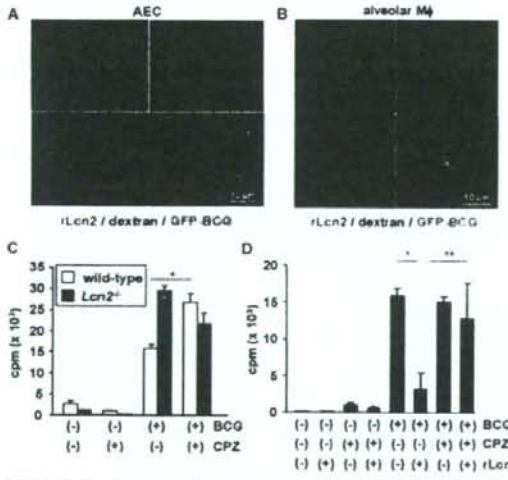

FIGURE 7. Requirement of Lcn2 incorporation for the inhibition of intracellular BCG growth. *A*, GFP-expressing BCG (green) infected alveolar epithelial cells were cultured with dextran (25 μg/ml; blue) and fluorescein-labeled rLcn2 (15 μg/ml; red) for 6 h. The cells were then washed, fixed with 4% PFA, and analyzed by confocal microscopy. Data are representative of three independent experiments. *B*, GFP-expressing BCG (green)-infected alveolar macrophages were cultured with dextran (25 μg/ml; blue) and fluorescein-labeled rLcn2 (15 μg/ml; red) for 6 h. The cells were then washed, fixed with 4% PFA for 5 min, and analyzed by confocal microscopy. *C*, Wild-type and *Lcn2*$^{-/-}$ AECs were seeded onto 96-well plates and infected with BCG (2×10^5 CFU) for 6 h. After extensive washing, the cells were cultured with CPZ (10 μM) and [^{3}H]uracil for 48 h. The [^{3}H]uracil incorporation was then measured. Data are presented as means ± SD of triplicate samples, and are representative of two independent experiments. *, $p < 0.01$. *D*, *Lcn2*$^{-/-}$ AECs were seeded onto 96-well plates, and infected with BCG for 6 h. After washing, the cells were cultured with CPZ for 30 min and then cultured with rLcn2 (20 μg/ml) and [^{3}H]uracil for 48 h. The [^{3}H]uracil incorporation was measured. Data are presented as means ± SD of triplicate samples, and are representative of two independent experiments. * or ** indicate a significant difference among groups, ANOVA posthoc Scheffe, *, $p < 0.005$; **, $p < 0.05$.

endocytosis of Lcn2 using CPZ after BCG infection. Addition of CPZ resulted in increased BCG growth in wild-type AECs, but not in *Lcn2*$^{-/-}$ cells (Fig. 7*C*). We also analyzed the effects of the endocytosis inhibitor on rLcn2-mediated inhibition of BCG growth (Fig. 7*D*). Addition of CPZ abolished Lcn2-mediated inhibition of [^{3}H]uracil incorporation in both wild-type and *Lcn2*$^{-/-}$ cells. Cytochalasin B, which also blocks endocytosis, had similar effects to those of CPZ on Lcn2-mediated inhibition of intracellular BCG growth (data not shown). These findings indicate that endocytosed Lcn2 inhibits the intracellular growth of BCG in AECs.

Discussion

Lcn2 has a variety of putative functions, as evident from its many different names such as neutrophil gelatinase-associated lipocalin, uterocalin, 24p3, and siderocalin (12, 13, 16, 19). In the context of its function in host defense, a structural study of the Lcn2 protein revealed that it associates with enterobactin-type bacterial siderophores (16). Subsequently, Lcn2 was shown to bind to several types of siderophores such as carboxy-mycobactin and bacillibactin (20, 21). In addition, Lcn2 has been proposed to bind to an as-yet unknown mammalian siderophore (18, 34). Thus, Lcn2 has the ability to bind to a variety of types of siderophores. Furthermore, Lcn2 has been shown to inhibit the growth of *E. coli* through sequestration of iron uptake (22, 23). The present study has demonstrated that Lcn2 also participates in the inhibition of mycobacterial growth through similar mechanisms to those against *E. coli*. Indeed, Lcn2 has been shown to associate with the mycobacteria-derived hydrophilic siderophore carboxy-mycobactin (21). In accordance with our results, Lcn2 has been shown to be secreted from neutrophils during *M. tuberculosis* infection and inhibit their growth (35). Lcn2 was originally identified as a molecule that is secreted from neutrophils, which are rapidly recruited to *M. tuberculosis*-infected lungs. Therefore, neutrophils are presumably the source of Lcn2 as well as alveolar macrophages and epithelial cells during *M. tuberculosis* infection.

Regarding the high sensitivity of *Lcn2*$^{-/-}$ mice to *M. tuberculosis* infection, it is noteworthy that *Lcn2*$^{-/-}$ alveolar epithelial cells, but not macrophages, contained increased numbers of *M. tuberculosis* at the early phase of the infection, as evaluated by histopathological and immunohistochemical analyses. This finding was unexpected, because successful in vivo detection of mycobacteria in respiratory epithelial cells in wild-type mice has only been achieved through analyses of mycobacterial DNA or use of electron microscopy, even though mycobacteria have been shown to invade epithelial cells as well as macrophages in vitro (6, 9, 36). In addition, *Lcn2*$^{-/-}$ alveolar epithelial cells, but not macrophages, exhibited defective inhibition of intracellular mycobacterial growth, suggesting that impaired inhibition of mycobacterial growth in alveolar epithelial cells due to the absence of Lcn2 may be a major cause of the high susceptibility *Lcn2*$^{-/-}$ mice to *M. tuberculosis* infection. Given that mycobacteria were easily detected in the alveolar epithelial cell layers by a typical histological approach in the absence of Lcn2 and the increased mycobacterial growth was observed in *Lcn2*$^{-/-}$ epithelial cells, but not in macrophages, epithelial cells may play an important role in the host immune responses against respiratory infection with *M. tuberculosis*.

Mycobacteria replicate within cells in vivo, and several lines of evidence indicate that mycobactin-mediated iron uptake is a prerequisite for intracellular mycobacterial growth (27, 29). Consistent with previous studies (18, 19), our findings indicated that Lcn2 is internalized into alveolar epithelial cells via endocytosis. Furthermore, addition of rLcn2 effectively inhibited intracellular mycobacterial growth in AECs, and this effect was abolished by endocytosis inhibitors. At present, it remains unclear how mycobacteria take up iron within epithelial cells using mycobactin. First, it is apparent that mycobacteria exist in the phagosome of macrophages. However, the subcellular localization of mycobacteria within epithelial cells has not been established, although mycobacteria have been shown to be localized in endosomes or macropinosomes (37, 38). Our results revealed colocalization of mycobacteria and dextran, indicating that mycobacteria exist in the endosome-like vacuole within epithelial cells. Second, it remains obscure whether mycobacteria secrete water-soluble carboxy-mycobactin into the cytoplasm to bind the cytosolic iron. It is also obscure how endocytosed Lcn2 approaches the carboxy-mycobactin/iron complexes within the cells. Given that Lcn2 and mycobacteria are colocalized within the endosome-like structure, it is possible that mycobacteria take up the iron entering the endosome using mycobactin, and endocytosed Lcn2, in turn, binds to the carboxy-mycobactin/iron complexes, thereby blocking iron acquisition by mycobacteria. Further studies are required to clarify the precise mechanisms for the interaction between Lcn2 and mycobacteria-derived carboxy-mycobactin.

In alveolar macrophages, the absence of Lcn2 did not affect the sensitivity to mycobacterial infection. This may be due to the differential localization of mycobacteria in epithelial cells and macrophages. Lcn2 may colocalize with mycobacteria in epithelial

cells, indicating that mycobacteria exist within the endosome-like structure. In contrast, mycobacteria were localized within the phagosome in macrophages, leading to distinct localizations of Lcn2 and mycobacteria in macrophages. Alternatively, macrophages are professional cells that kill intracellular bacteria by producing several macrophage-specific anti-microbial mediators, including NO synthase and Nramp1 (39–41). These mediators may compensate the Lcn2 deficiency in macrophages. In contrast, they are not expressed in epithelial cells, resulting in the high sensitivity to mycobacterial infection in the absence of Lcn2. Thus, in alveolar epithelial cells, Lcn2 may be a major factor that mediates host resistance to mycobacterial infection.

Our results highlight a novel innate host defense system that inhibits mycobacterial infection at the respiratory mucosal surface. We would like to propose the following scenario with regard to the function of Lcn2. Lcn2 is secreted into the alveolar space by alveolar macrophages and epithelial cells during the early phase of respiratory mycobacterial infection. Lcn2 presumably inhibits mycobacterial growth within the alveolar space. In addition, Lcn2 is internalized into the alveolar epithelial cells, which are invaded by mycobacteria, and inhibits mycobacterial growth by sequestering iron uptake. This leads to a reduction in the number of infected mycobacteria at the early phase of infection, which may help to create sufficient time for effective activation of anti-mycobacterial innate and adaptive immune responses. Thus, respiratory epithelial cells play an active role in the resistance to mycobacterial infection, in addition to their functions as physical barriers and secretors of anti-bacterial mediators.

Acknowledgments

We thank I. Sugawara for providing the *M. tuberculosis* H37Rv, Y. Yamada and K. Takeda for technical assistance, and M. Kurata and M. Yasuda for secretarial assistance.

Disclosures

The authors have no financial conflict of interest.

References

1. North, R. J., and Y. J. Jung. 2004. Immunity to tuberculosis. *Annu. Rev. Immunol.* 22: 599–623.
2. Kaufmann, S. H. 2006. Tuberculosis: back on the immunologists' agenda. *Immunity* 24: 351–357.
3. Quesniaux, V., C. Fremond, M. Jacobs, S. Parida, D. Nicolle, V. Yeremeev, F. Bihl, F. Erard, T. Botha, M. Drennan, et al. 2004. Toll-like receptor pathways in the immune responses to mycobacteria. *Microbes Infect.* 6: 946–959.
4. Fremond, C. M., V. Yeremeev, D. M. Nicolle, M. Jacobs, V. F. Quesniaux, and B. Ryffel. 2004. Fatal *Mycobacterium tuberculosis* infection despite adaptive immune response in the absence of MyD88. *J. Clin. Invest.* 114: 1790–1799.
5. Aoki, K., S. Matsumoto, Y. Hirayama, T. Wada, Y. Ozeki, M. Niki, P. Domenech, K. Umemori, S. Yamamoto, A. Mineda, et al. 2004. Extracellular mycobacterial DNA-binding protein 1 participates in mycobacterium-lung epithelial cell interaction through hyaluronic acid. *J. Biol. Chem.* 279: 39798–39806.
6. Teitelbaum, R., W. Schubert, L. Gunther, Y. Kress, F. Macaluso, J. W. Pollard, D. N. McMurray, and B. R. Bloom. 1999. The M cell as a portal of entry to the lung for the bacterial pathogen *Mycobacterium tuberculosis*. *Immunity* 10: 641–651.
7. Bermudez, L. E., and F. J. Sangari. 2001. Cellular and molecular mechanisms of internalization of mycobacteria by host cells. *Microbes Infect.* 3: 37–42.
8. Bermudez, L. E., F. J. Sangari, P. Kolonoski, M. Petrofsky, and J. Goodman. 2002. The efficiency of the translocation of *Mycobacterium tuberculosis* across a bilayer of epithelial and endothelial cells as a model of the alveolar wall is a consequence of transport within mononuclear phagocytes and invasion of alveolar epithelial cells. *Infect. Immun.* 70: 140–146.
9. Hernandez-Pando, R., M. Jeyanathan, G. Mengistu, D. Aguilar, H. Orozco, M. Harboe, G. A. Rook, and G. Bjune. 2000. Persistence of DNA from *Mycobacterium tuberculosis* in superficially normal lung tissue during latent infection. *Lancet* 356: 2133–2138.
10. Ferguson, J. S., and L. S. Schlesinger. 2000. Pulmonary surfactant in innate immunity and the pathogenesis of tuberculosis. *Tuber. Lung Dis.* 80: 173–184.
11. Kjeldsen, L., J. B. Cowland, and N. Borregaard. 2000. Human neutrophil gelatinase-associated lipocalin and homologous proteins in rat and mouse. *Biochim. Biophys. Acta* 1482: 272–283.
12. Devireddy, L. R., J. G. Teodoro, F. A. Richard, and M. R. Green. 2001. Induction of apoptosis by a secreted lipocalin that is transcriptionally regulated by IL-3 deprivation. *Science* 293: 829–834.
13. Kjeldsen, L., A. H. Johnsen, H. Sengelov, and N. Borregaard. 1993. Isolation and primary structure of NGAL, a novel protein associated with human neutrophil gelatinase. *J. Biol. Chem.* 268: 10425–10432.
14. Flower, D. R., A. C. North, and T. K. Attwood. 1991. Mouse oncogene protein 24p3 is a member of the lipocalin protein family. *Biochem. Biophys. Res. Commun.* 180: 69–74.
15. Liu, Q., J. Ryon, and M. Nilsen-Hamilton. 1997. Uterocalin: a mouse acute phase protein expressed in the uterus around birth. *Mol. Reprod. Dev.* 46: 507–514.
16. Goetz, D. H., M. A. Holmes, N. Borregaard, M. E. Bluhm, K. N. Raymond, and R. K. Strong. 2002. The neutrophil lipocalin NGAL is a bacteriostatic agent that interferes with siderophore-mediated iron acquisition. *Mol. Cell* 10: 1033–1043.
17. Nilsen-Hamilton, M., Q. Liu, J. Ryon, L. Bendickson, P. Lepont, and Q. Chang. 2003. Tissue involution and the acute phase response. *Ann. NY Acad. Sci.* 995: 94–108.
18. Devireddy, L. R., C. Gazin, X. Zhu, and M. R. Green. 2005. A cell-surface receptor for lipocalin 24p3 selectively mediates apoptosis and iron uptake. *Cell* 123: 1293–1305.
19. Yang, J., D. Goetz, J. Y. Li, W. Wang, K. Mori, D. Setlik, T. Du, H. Erdjument-Bromage, P. Tempst, R. Strong, and J. Barasch. 2002. An iron delivery pathway mediated by a lipocalin. *Mol. Cell* 10: 1045–1056.
20. Abergel, R. J., M. K. Wilson, J. F. Arceneaux, T. M. Hoette, R. K. Strong, B. R. Byers, and K. N. Raymond. 2006. Anthrax pathogen evades the mammalian immune system through stealth siderophore production. *Proc. Natl. Acad. Sci. USA* 103: 18499–18503.
21. Holmes, M. A., W. Paulsene, X. Jide, C. Ratledge, and R. K. Strong. 2005. Siderocalin (Lcn 2) also binds carboxymycobactins, potentially defending against mycobacterial infections through iron sequestration. *Structure* 13: 29–41.
22. Flo, T. H., K. D. Smith, S. Sato, D. J. Rodriguez, M. A. Holmes, R. K. Strong, S. Akira, and A. Aderem. 2004. Lipocalin 2 mediates an innate immune response to bacterial infection by sequestrating iron. *Nature* 432: 917–921.
23. Berger, T., A. Togawa, G. S. Duncan, A. J. Elia, A. You-Ten, A. Wakeham, H. E. Fong, C. C. Cheung, and T. W. Mak. 2006. Lipocalin 2-deficient mice exhibit increased sensitivity to *Escherichia coli* infection but not to ischemia-reperfusion injury. *Proc. Natl. Acad. Sci. USA* 103: 1834–1839.
24. Smith, K. D. 2007. Iron metabolism at the host pathogen interface: lipocalin 2 and the pathogen-associated iroA gene cluster. *Int. J. Biochem. Cell Biol.* 39: 1776–1780.
25. Houben, E. N., L. Nguyen, and J. Pieters. 2006. Interaction of pathogenic mycobacteria with the host immune system. *Curr. Opin. Microbiol.* 9: 76–85.
26. De Voss, J. J., K. Rutter, B. G. Schroeder, and C. E. Barry, 3rd. 1999. Iron acquisition and metabolism by mycobacteria. *J. Bacteriol.* 181: 4443–4451.
27. De Voss, J. J., K. Rutter, B. G. Schroeder, H. Su, Y. Zhu, and C. E. Barry, 3rd. 2000. The salicylate-derived mycobactin siderophores of *Mycobacterium tuberculosis* are essential for growth in macrophages. *Proc. Natl. Acad. Sci. USA* 97: 1252–1257.
28. Gobin, J., and M. A. Horwitz. 1996. Exochelins of *Mycobacterium tuberculosis* remove iron from human iron-binding proteins and donate iron to mycobactins in the *M. tuberculosis* cell wall. *J. Exp. Med.* 183: 1527–1532.
29. Luo, M., E. A. Fadeev, and J. T. Groves. 2005. Mycobactin-mediated iron acquisition within macrophages. *Nat. Chem. Biol.* 1: 149–153.
30. Jat, P. S., M. D. Noble, P. Ataliotis, Y. Tanaka, N. Yannoutsos, L. Larsen, and D. Kioussis. 1991. Direct derivation of conditionally immortal cell lines from an H-2Kb-tsA58 transgenic mouse. *Proc. Natl. Acad. Sci. USA* 88: 5096–5100.
31. Whitehead, R. H., P. E. VanEeden, M. D. Noble, P. Ataliotis, and P. S. Jat. 1993. Establishment of conditionally immortalized epithelial cell lines from both colon and small intestine of adult H-2Kb-tsA58 transgenic mice. *Proc. Natl. Acad. Sci. USA* 90: 587–591.
32. deMello, D. E., S. Mahmoud, P. J. Padfield, and J. W. Hoffmann. 2000. Generation of an immortal differentiated lung type-II epithelial cell line from the adult H-2Kb/tsA58 transgenic mouse. *In Vitro Cell. Dev. Biol. Anim.* 36: 374–382.
33. Rook, G. A., B. R. Champion, J. Steele, A. M. Varey, and J. L. Stanford. 1985. I-A restricted activation by T cell lines of anti-tuberculosis activity in murine macrophages. *Clin. Exp. Immunol.* 59: 414–420.
34. Mori, K., H. T. Lee, D. Rapoport, I. R. Drexler, K. Foster, J. Yang, K. M. Schmidt-Ott, X. Chen, J. Y. Li, S. Weiss, et al. 2005. Endocytic delivery of lipocalin-siderophore-iron complex rescues the kidney from ischemia-reperfusion injury. *J. Clin. Invest.* 115: 610–621.
35. Martineau, A. R., S. M. Newton, K. A. Wilkinson, B. Kampmann, B. M. Hall, N. Nawroly, G. E. Packe, R. N. Davidson, C. J. Griffiths, and R. J. Wilkinson. 2007. Neutrophil-mediated innate immune resistance to mycobacteria. *J. Clin. Invest.* 117: 1988–1994.
36. Sato, K., H. Tomioka, T. Shimizu, T. Gonda, F. Ota, and C. Sano. 2002. Type II alveolar cells play roles in macrophage-mediated host innate resistance to pulmonary mycobacterial infections by producing proinflammatory cytokines. *J. Infect. Dis.* 185: 1139–1147.
37. Bermudez, L. E., and J. Goodman. 1996. *Mycobacterium tuberculosis* invades and replicates within type II alveolar cells. *Infect. Immun.* 64: 1400–1406.
38. Garcia-Perez, B. E., R. Mondragon-Flores, and J. Luna-Herrera. 2003. Internalization of *Mycobacterium tuberculosis* by macropinocytosis in non-phagocytic cells. *Microb. Pathog.* 35: 49–55.
39. Adams, D. O., and T. A. Hamilton. 1984. The cell biology of macrophage activation. *Annu. Rev. Immunol.* 2: 283–318.
40. MacMicking, J., Q. W. Xie, and C. Nathan. 1997. Nitric oxide and macrophage function. *Annu. Rev. Immunol.* 15: 323–350.
41. Govoni, G., and P. Gros. 1998. Macrophage NRAMP1 and its role in resistance to microbial infections. *Inflamm. Res.* 47: 277–284.

JOURNAL OF BACTERIOLOGY, May 2008, p. 3613–3621 Vol. 190, No. 10
0021-9193/08/$08.00+0 doi:10.1128/JB.01850-07

Structural Analysis and Biosynthesis Gene Cluster of an Antigenic Glycopeptidolipid from *Mycobacterium intracellulare*▽†

Nagatoshi Fujiwara,[1]* Noboru Nakata,[2] Takashi Naka,[1,3] Ikuya Yano,[3] Matsumi Doe,[4] Delphi Chatterjee,[5] Michael McNeil,[5] Patrick J. Brennan,[5] Kazuo Kobayashi,[6] Masahiko Makino,[2] Sohkichi Matsumoto,[1] Hisashi Ogura,[7] and Shinji Maeda[8]

Department of Host Defense[1] and Virology,[7] Osaka City University Graduate School of Medicine, Osaka 545-8585, Japan; Department of Microbiology, Leprosy Research Center, National Institute of Infectious Diseases, Tokyo 189-0002, Japan[2]; Japan BCG Laboratory, Tokyo 204-0022, Japan[3]; Department of Chemistry, Graduate School of Science, Osaka City University, Osaka 558-8585, Japan[4]; Department of Microbiology, Immunology and Pathology, Colorado State University, Colorado 80523[5]; Department of Immunology, National Institute of Infectious Diseases, Tokyo 162-8640, Japan[6]; and Molecular Epidemiology Division, Mycobacterium Reference Center, The Research Institute of Tuberculosis, Japan Anti-Tuberculosis Association, Tokyo 204-8533, Japan[8]

Received 24 November 2007/Accepted 1 March 2008

***Mycobacterium avium-Mycobacterium intracellulare* complex (MAC) is the most common isolate of nontuberculous mycobacteria and causes pulmonary and extrapulmonary diseases. MAC species can be grouped into 31 serotypes by the epitopic oligosaccharide structure of the species-specific glycopeptidolipid (GPL) antigen. The GPL consists of a serotype-common fatty acyl peptide core with 3,4-di-*O*-methyl-rhamnose at the terminal alaninol and a 6-deoxy-talose at the *allo*-threonine and serotype-specific oligosaccharides extending from the 6-deoxy-talose. Although the complete structures of 15 serotype-specific GPLs have been defined, the serotype 16-specific GPL structure has not yet been elucidated. In this study, the chemical structure of the serotype 16 GPL derived from *M. intracellulare* was determined by using chromatography, mass spectrometry, and nuclear magnetic resonance analyses. The result indicates that the terminal carbohydrate epitope of the oligosaccharide is a novel *N*-acyl-dideoxy-hexose. By the combined linkage analysis, the oligosaccharide structure of serotype 16 GPL was determined to be 3-2′-methyl-3′-hydroxy-4′-methoxy-pentanoyl-amido-3,6-dideoxy-β-hexose-(1→3)-4-*O*-methyl-α-L-rhamnose-(1→3)-α-L-rhamnose-(1→3)-α-L-rhamnose-(1→2)-6-deoxy-α-L-talose. Next, the 22.9-kb serotype 16-specific gene cluster involved in the glycosylation of oligosaccharide was isolated and sequenced. The cluster contained 17 open reading frames (ORFs). Based on the similarity of the deduced amino acid sequences, it was assumed that the ORF functions include encoding three glycosyltransferases, an acyltransferase, an aminotransferase, and a methyltransferase. An *M. avium* serotype 1 strain was transformed with cosmid clone no. 253 containing *gtfB-drrC* of *M. intracellulare* serotype 16, and the transformant produced serotype 16 GPL. Together, the ORFs of this serotype 16-specific gene cluster are responsible for the biosynthesis of serotype 16 GPL.**

Mycobacterial diseases, such as tuberculosis and infection due to nontuberculous mycobacteria (NTM), are still among the most serious infectious diseases in the world. The incidence is increasing because of the spread of drug-resistant mycobacteria and the human immunodeficiency virus (HIV) infection/AIDS epidemic (16, 17, 30). *Mycobacterium avium-Mycobacterium intracellulare* complex (MAC) is the most common among isolates of NTM and is distributed ubiquitously in the environment. MAC causes pulmonary and extrapulmonary diseases in both immunocompromised and immunocompetent hosts. It affects primarily patients with advanced HIV infection. MAC includes at least two mycobacterial species, *M. avium* and *M. intracellulare*, that cannot be differentiated on the basis of traditional physical and biochemical tests (1, 41).

* Corresponding author. Mailing address: Department of Host Defense, Osaka City University Graduate School of Medicine, 1-4-3 Asahi-machi, Abeno-ku, Osaka 545-8585, Japan. Phone: 81 6 6645 3746. Fax: 81 6 6645 3747. E-mail: fujiwara@med.osaka-cu.ac.jp.

† Supplemental material for this article may be found at http://jb.asm.org/.

Published ahead of print on 7 March 2008.

The cell envelope of mycobacteria is a complex and unusual structure. The key feature of this structure is an extraordinarily high lipid concentration (6, 10). To better understand the pathogenesis of MAC infection, it is necessary to elucidate the molecular structure and biochemical features of the lipid components. Among MAC lipids, the glycopeptidolipid (GPL) is of particular importance, because it shows not only serotype-specific antigenicity but also immunomodulatory activities in the host immune responses (2, 9, 23). Structurally, GPLs are composed of two parts, a tetrapeptide-amino alcohol core and a variable oligosaccharide (OSE). C_{26}-C_{34} fatty acyl-D-phenylalanine-D-*allo*-threonine-D-alanine-L-alaninol (D-Phe-D-*allo*-Thr-D-Ala-L-alaninol) is further linked with 6-deoxy talose (6-d-Tal) and 3,4-di-*O*-methyl rhamnose (3,4-di-*O*-Me-Rha) at D-*allo*-Thr and the terminal L-alaninol, respectively. This type of core GPL is found in all subspecies of MAC, shows a common antigenicity, and is further glycosylated at 6-d-Tal to form a serotype-specific OSE.

At present, 31 distinct serotype-specific GPLs have been identified serologically and chromatographically (9). Although the standard technique for differentiation of MAC subspecies

has been serotyping based on the OSE residue of its GPL, the complete structures of only 15 GPLs have been defined. In addition to the chemical structures of various GPLs, genes encoding the glycosylation pathways in the biosynthesis of GPL have been identified and characterized (12, 21, 31). Epidemiological studies have shown that MAC serotypes 4 and 8 are the most frequently isolated from patients, and MAC serotype 16 is one of the next most common groups (32, 40). It has been suggested that the serotypes of MAC isolates participate in their virulence (29), and thus, understanding of the structure-pathogenicity relationship of GPLs is necessary. In the present study, we demonstrate the complete OSE structure of the GPL derived from serotype 16 MAC (*M. intracellulare*), which has a unique terminal-acylated-amido sugar, and we characterized the serotype 16 GPL-specific gene cluster involved in the glycosylation of carbohydrates.

MATERIALS AND METHODS

Bacterial strains and preparation of GPL. *M. intracellulare* serotype 16 strain ATCC 13950^T (NF 115) was purchased from the American Type Culture Collection (Manassas, VA). Three clinical isolates of *M. intracellulare* serotype 16 (NF 116 and 117) and *M. avium* serotype 1 (NF 113) were maintained in The Research Institute of Tuberculosis, Japan Anti-Tuberculosis Association. The preparation of GPL was performed as described previously (18, 24, 26). Briefly, each strain of *M. intracellulare* serotype 16 was grown in Middlebrook 7H9 broth (Difco Laboratories, Detroit, MI) with 0.5% glycerol and 10% Middlebrook oleic acid-albumin-dextrose-catalase enrichment (Difco) at 37°C for 2 to 3 weeks. The heat-killed bacteria were sonicated, and crude lipids were extracted with chloroform-methanol (2:1, vol/vol). The extracted lipids were dried and hydrolyzed with 0.2 N sodium hydroxide in methanol at 37°C for 2 h. After neutralization with 6 N hydrochloric acid, alkaline-stable lipids were partitioned by a two-layer system of chloroform-methanol (2:1, vol/vol) and water. The organic phase was recovered, evaporated, and precipitated with acetone to remove any acetone-insoluble components containing phospholipids and glycolipids. The supernatant was collected by centrifugation, dried, and then treated with a Sep-Pak silica cartridge (Waters Corporation, Milford, MA) with washing (chloroform-methanol, 95:5, vol/vol) and elution (chloroform-methanol, 1:1, vol/vol) for partial purification. GPL was completely purified by preparative thin-layer chromatography (TLC) of Silica Gel G (20 by 20 cm, 250 μm; Uniplate; Analtech, Inc., Newark, DE). The TLC plate was repeatedly developed with chloroform-methanol-water (65:25:4 and 60:16:2, vol/vol/vol) until a single spot was obtained. After exposure of the TLC plate to iodine vapor, the GPL band was marked, and then, the silica gels were scraped off and the GPL was eluted with chloroform-methanol (2:1, vol/vol).

Preparation of OSE moiety. β elimination of GPL was performed with alkaline borohydride, and the OSE elongated from *O*-allo-Thr was released as described previously (18, 24). Briefly, the GPL was dissolved in ethanol, and an equal volume of 10 mg/ml sodium borohydride or borodeuteride in 0.5 N sodium hydroxide was added and then stirred at 60°C for 16 h. The reaction mixture was decationized with Dowex 50W-X8 beads (Dow Chemical Company, Midland, MI), collected, and evaporated under nitrogen to remove boric acid. The dried residue was partitioned in two layers of chloroform-methanol (2:1, vol/vol) and water. The upper aqueous phase was recovered and evaporated. In these processes, the serotype 16-specific OSE was purified as an oligoglycosyl alditol.

MALDI-TOF and MALDI-TOF/TOF MS analyses. The molecular species of the intact GPL was detected by matrix-assisted laser desorption ionization–time of flight mass spectrometry (MALDI-TOF MS) with an Ultraflex II (Bruker Daltonics, Billerica, MA). The GPL was dissolved in chloroform-methanol (2:1, vol/vol) at a concentration of 1 mg/ml, and 1 μl was applied directly to the sample plate, and then 1 μl of 10 mg/ml 2,5-dihydroxybenzoic acid in chloroform-methanol (1:1, vol/vol) was added as a matrix. The intact GPL was analyzed in the reflectron mode with an accelerating voltage operating in a positive mode of 20 kV (5). Then the fragment pattern of the OSE was analyzed with MALDI-TOF/TOF MS. The OSE was dissolved in ethanol-water (3:7, vol/vol), and the matrix was 10 mg/ml 2,5-dihydroxybenzoic acid in ethanol-water (3:7, vol/vol). The OSE and the matrix were applied to the sample plate according to the method for intact GPL and analyzed in the lift-lift mode.

GC and GC-MS analyses of carbohydrates and *N*-acylated short-chain fatty acid. To determine the glycosyl composition and linkage position, gas chromatography (GC) and GC-MS analyses of partially methylated alditol acetate derivatives were performed. Perdeuteromethylation was conducted by the modified procedure of Hakomori as described previously (18, 20). Briefly, the dried OSE was dissolved with a mixture of dimethyl sulfoxide and sodium hydroxide, and deuteromethyl iodide was added. The reaction mixture was stirred at room temperature for 15 min and then water and chloroform were added. The chloroform-containing perdeuteromethylated OSE layer was collected, washed with water two times, and then completely evaporated. Partially deuteromethylated alditol acetates were prepared from perdeuteromethylated OSE by hydrolysis with 2 N trifluoroacetic acid at 120°C for 2 h, reduction with 10 mg/ml sodium borodeuteride at 25°C for 2 h, and acetylation with acetic anhydride at 100°C for 1 h (8, 18, 25). To identify amino-linked fatty acids, acidic methanolysis of serotype 16 GPL was performed with 1.25 M hydrogen chloride in methanol (Sigma-Aldrich, St. Louis, MO) at 100°C for 90 min, and the fatty acid methyl esters were extracted with *n*-hexane under the cooled ice. GC was performed using a 5890 series II gas chromatograph (Hewlett Packard, Avondale, PA) equipped with a fused SPB-1 capillary column (30 m, 0.25-mm inner diameter; Supelco Inc., Bellefonte, PA). Helium was used for electron impact (EI)-MS and isobutane for chemical ionization (CI)-MS as a carrier gas. A JMS SX102A double-focusing mass spectrometer (JEOL, Tokyo, Japan) was connected to the gas chromatograph as a mass detector. The molecular separator and the ion source energy were 70 eV for EI and 30 eV for CI, and the accelerating voltage was 8 kV. The D- and L-configurations of Rha residues were determined by comparative GC-MS analysis of trimethylsilylated (*S*)-(+)-sec-butyl glycosides and (*R*)-(−)-sec-butyl glycosides prepared from an authentic standard L-Rha (19).

NMR analysis of GPL. The GPL was dissolved in chloroform-d ($CDCl_3$)-methanol-d_4 (CD_3OD) (2:1, vol/vol). To define the anomeric configurations of each glycosyl residue, ^1H and ^{13}C nuclear magnetic resonance (NMR) was employed. Both homonuclear correlation spectrometry (COSY) and ^1H-detected [^1H, ^{13}C] heteronuclear multiple-quantum correlation (HMQC) were recorded with a Bruker Avance-600 (Bruker BioSpin Corp., Billerica, MA), as described previously (9, 18, 24, 34).

Construction of *M. intracellulare* serotype 16 cosmid library. A cosmid library of *M. intracellulare* serotype 16 strain ATCC 13950^T was constructed as described previously (18). Bacterial cells were disrupted mechanically, and genomic DNA was extracted with phenol-chloroform and then precipitated with ethanol. Genomic DNA randomly sheared into 30- to 50-kb fragments in the extraction process was fractionated and electroeluted from agarose gels using a Takara Recochip (Takara, Kyoto, Japan). These DNA fragments were rendered blunt ended using T4 DNA polymerase and deoxynucleoside triphosphates and then were ligated to dephosphorylated arms of pYUB412 (XbaI-EcoRV and EcoRV-XbaI), which were the kind gifts of William R. Jacobs, Jr. (Department of Microbiology and Immunology, Albert Einstein College of Medicine, Bronx, NY). The cosmid vector pYUB412 is an *Escherichia coli-Mycobacterium* shuttle vector with the *int-attP* sequence for integration into a mycobacterial chromosome, *oriE* for replication in *E. coli*, a hygromycin resistance gene, and an ampicillin resistance gene. After in vitro packaging using Gigapack III Gold extracts (Stratagene, La Jolla, CA), recombinant cosmids were introduced into *E. coli* STBL2 [F$^-$ *mcrA* Δ(*mcrBC-hsdRMS-mrr*) *recA1 endA1 lon gyrA96 thi supE44 relA1* Δ(*lac-proAB*)] and stored at −80°C in 50% glycerol.

Isolation of cosmid clones carrying biosynthesis gene cluster of serotype 16 GPL and sequence analysis. Isolation of DNA from *E. coli* transductants was performed as described by Supply et al., with modifications (39). The colonies were picked, transferred to a 1.5-ml tube containing 50 μl of water, and then heated at 98°C for 5 min. After centrifugation at 14,000 rpm for 5 min, the supernatant was used as the PCR template. PCR was used to isolate cosmid clones carrying the rhamnosyltransferase (*rtfA*) gene with primers rtfA-F (5′-TTTGGAGCGACGAGTTCATC-3′) and rtfA-R (5′-GTCGTAGTTGACCACGCCGAC-3′). *rtfA* encodes an enzyme responsible for the transfer of Rha to 6-d-Tal in OSE (14, 31). The insert of cosmid clone no. 253 was sequenced using a BigDye Terminator, version 3.1, cycle sequencing kit (Applied Biosystems, Foster City, CA) and an ABI Prism 310 gene analyzer (Applied Biosystems). The putative function of each open reading frame (ORF) was identified by similarity searches between the deduced amino acid sequences and known proteins using BLAST (http://www.ncbi.nlm.nih.gov/BLAST/) and FramePlot (http://www.nih.go.jp/~jun/cgi-bin/frameplot.pl) with the DNASIS computer program (Hitachi Software Engineering, Yokohama, Japan).

Transformation of *M. avium* serotype 1 strain with cosmid clone no. 253. An *M. avium* serotype 1 strain (NF113) was transformed with pYUB412-cosmid clone no. 253 by electroporation, and hygromycin-resistant colonies were iso-

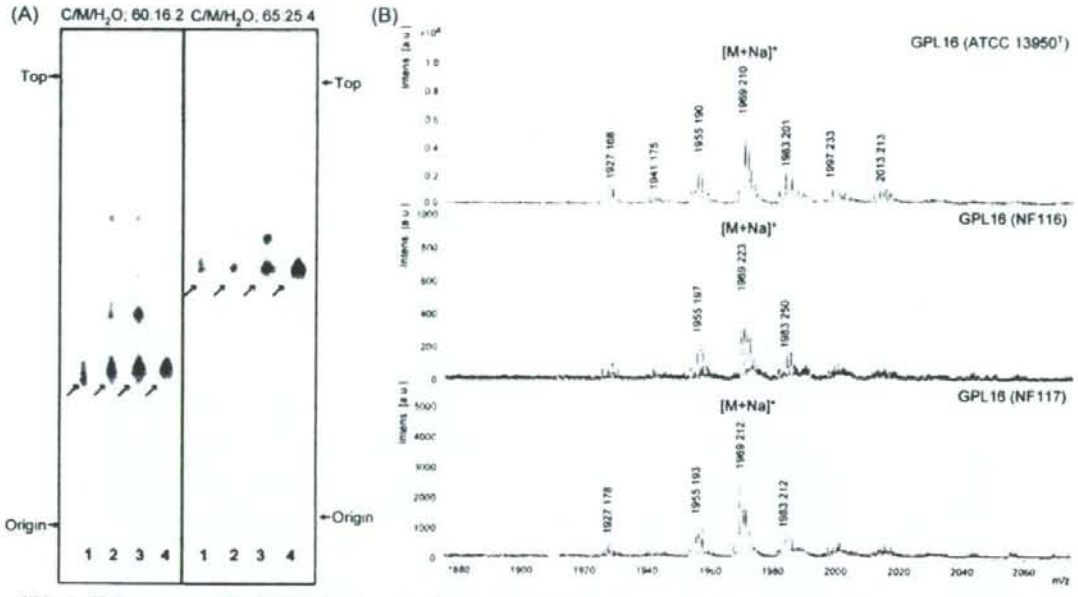

FIG. 1. TLC patterns and MALDI-TOF MS spectra of serotype 16 GPI. (A) Serotype 16 GPI purified from *M. intracellulare* ATCC 13950[T] (NF 115) and the alkaline-stable lipids derived from ATCC 13950[T] and two clinical isolates (NF 116 and 117) from left to right were developed on TLC plates with solvent systems of chloroform-methanol-water (65:25:4 and 60:16:2, vol/vol/vol). (B) The MALDI-TOF MS spectra were acquired using 10 mg/ml 2,5-dihydroxybenzoic acid in chloroform-methanol (1:1, vol/vol) as a matrix, and the molecularly related ions were detected as $[M + Na]^+$ in positive mode. Intens., intensity; a.u., absorbance units.

lated. Alkaline-stable lipids were prepared, and productive GPLs were examined by TLC and MALDI-TOF MS analyses.

Nucleotide sequence accession number. The nucleotide sequence reported here has been deposited in the NCBI GenBank database under accession no. AB355138.

RESULTS

Purification and molecular weight of intact GPLs. Serotype 16 GPL from *M. intracellulare* ATCC 13950[T] (NF 115) was detected as a spot by TLC, and the R_f values were 0.35 and 0.56 when developed with chloroform-methanol-water (60:16:2 and 65:25:4, vol/vol/vol, respectively). Two clinical isolates of *M. intracellulare*, NF 116 and 117, had serotype 16 GPLs that showed the same R_f values as the serotype 16 GPL derived from strain ATCC 13950[T]. The serotype 16 GPL of *M. intracellulare* strain ATCC 13950[T] was purified repeatedly by TLC and was shown as a single spot by TLC (Fig. 1A). The MALDI-TOF MS spectra of each serotype 16 GPL showed *m/z* 1969 for $[M+Na]^+$ as the main molecularly related ion in positive mode, with the homologous ions differing by 14 mass units at 1,955 and 1,983 (Fig. 1B). As a result, the main molecular weight of serotype 16 GPL was 1,946, which implied that it has a novel carbohydrate chain elongated from *ribitol*-1Hr.

Carbohydrate composition of serotype 16 OSE. To determine the glycosyl compositions of serotype 16 OSE, alditol acetate derivatives of the serotype 16 GPL were analyzed by GC and GC-MS. The structurally defined serotype 4 GPL was used as a reference standard (9, 35). Comparison of the retention time and GC mass spectra (Fig. 2) with the alditol acetate derivatives of the serotype 16 GPL showed the presence of 3,4-di-*O*-Me-Rha, 4-*O*-Me-Rha, Rha, 6-d-Tal, and an unknown sugar residue (X1) in a ratio of approximately 1:1.2:1:1. The alditol acetate of X1 was eluted at a retention time of 29.3 min, greater than that of glucitol acetate on the SPB-1 column. The CI-MS spectrum of X1 was $[M+H]^+$ at *m/z* 520 as a parent ion and *m/z* 460 as a loss of 60 (acetate). The fragment ions of X1 sugar showed characteristic patterns in EI-MS. *m/z* 360 indicated the cleavage of C-3 and C-4, and *m/z* 300, 240, and 180 were fragmented with a loss of 60 (acetate). Similarly, *m/z* 374 indicated the cleavage of C-2 and C-3, and *m/z* 314 and 254 were fragmented with a loss of 60 (Fig. 3A and B). These results indicated that X1 was 3,6-dideoxy hexose (Hex). The odd molecular weight of X1, 519, and *m/z* 187, 127, and 59 implied the presence of one amido group esterified with a short-chain fatty acid, possibly. After methanolysis of serotype 16 GPL, the resultant fatty acid methyl esters were extracted carefully and analyzed by GC-MS. The EI-MS spectrum of a short-chain fatty acid methyl ester showed mass ions at *m/z* 176 ($[M]^+$), 145 ($[M-31]^+$), 117 ($[M-59]^+$), 99, 88, 85, and 59 (Fig. 3C) (33, 37). Taking the results together, X1 was structurally determined to be 3-2′-methyl-3′-hydroxy-4′-methoxy-pentanoyl-amido-3,6-dideoxy-Hex.

Glycosyl linkage and sequence of serotype 16 OSE. To determine the glycosyl linkage and sequence of the OSE, GC-MS of perdeuteromethylated alditol acetates and MALDI-TOF/TOF MS of the oligoglycosyl alditol from serotype 16 OSE

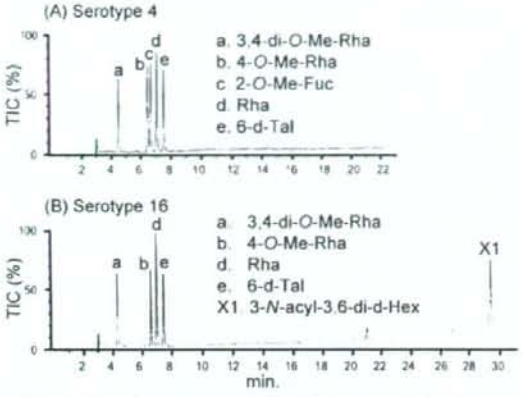

FIG. 2. Gas chromatograms of the alditol acetate derivatives from serotype 4 (A) and serotype 16 (B) GPIs. Total ion chromatograms (TIC) are shown. GC was performed on an SPB-1-fused silica column with a temperature program of 160°C for 2 min, followed by an increase of 4°C/min to 220°C, and holding at 220°C for 15 min. Comparison to the GC spectrum of serotype 4 GPI shows that serotype 16 GPI is composed of 3,4-di-*O*-Me-Rha, 4-*O*-Me-Rha, Rha, 6-d-Tal, and an unknown X1 sugar residue.

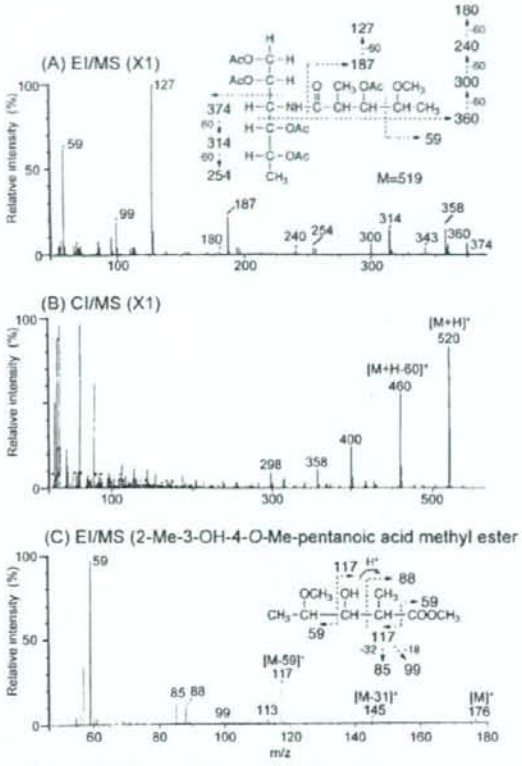

FIG. 3. EI-MS and CI-MS spectra of the alditol acetate derivative from X1 (A and B) and *N*-acylated-short-chain fatty acid methyl ester (C). The pattern of prominent fragment ions is illustrated. The GC column and condition were described in the legend for Fig. 2.

were performed. As shown in Fig. 4, the GC-MS spectra of perdeuteromethylated alditol acetates were assigned four major peaks, 1,3,4,5-tetra-*O*-deuteromethyl-2-*O*-acetyl-6-deoxytalitol (*m/z* 109, 132, 154, 167, and 214); 2,4-di-*O*-deuteromethyl-1,3,5-tri-*O*-acetyl-rhamnitol (*m/z* 121, 134, 205, 240, and 253); 2-*O*-deuteromethyl-4-*O*-methyl-1,3,5-tri-*O*-acetyl-rhamnitol (*m/z* 121, 131, 202, and 237); and 2,4-di-*O*-deuteromethyl-1,5-di-*O*-acetyl-3-2′-methyl-3′-*O*-deuteromethyl-4′methoxypentanoyl-deuteromethylamido-3,6-dideoxy-hexitol (*m/z* 121, 134, and 341). These results revealed that the 6-d-Tal residue was linked at C-2; Rha and 4-*O*-Me-Rha were linked at C-1 and C-3; and the nonreducing terminus, 3-2′-methyl-3′-hydroxy-4′-methoxy-pentanoyl-amido-3,6-dideoxy-Hex, was C-1 linked. The MALDI-TOF/TOF MS spectrum of the oligoglycosyl alditol from serotype 16 OSE afforded the expected molecular ions $[M+Na]^+$ at *m/z* 931, together with the characteristic mass increments in the series of glycosyloxonium ions formed on fragmentation at *m/z* 312, 472, 618, and 764 from the terminal sugar *N*-acyl-Hex to 6-d-Tal and at *m/z* 336, 482, and 642 from 6-d-Tal to *N*-acyl-Hex (Fig. 5). Rha residues were determined to be in the L absolute configuration by comparative GC-MS analyses of trimethylsilylated (*S*)-(+)-sec-butyl glycosides and (*R*)-(−)-sec-butylglycosides (see Fig. S1 in the supplemental material). Taken together, these results established the sequence and linkage arrangement 3-2′-methyl-3′-hydroxy-4′-methoxy-pentanoyl-amido-3,6-dideoxy-Hex-(1→3)-4-*O*-Me-Rha-(1→3)-L-Rha-(1→3)-L-Rha-(1→2)-6-d-Tal, exclusively.

NMR analysis of serotype 16 OSE. The ^{1}H NMR and ^{1}H-^{1}H COSY analyses of the serotype 16 GPI revealed six distinct anomeric protons with corresponding H1-H2 cross peaks in the low field region at δ4.93, 4.92, 4.92, 4.84, 4.65 ($J_{1,2}$ = 2 to 3 Hz, indicative of α-anomers) and 4.51 (a doublet, $J_{1,2}$ = 7.7 Hz, indicative of a β-hexosyl unit). When further analyzed by ^{1}H-detected [^{1}H, ^{13}C] two-dimensional HMQC, the anomeric protons resonating at δ4.93, 4.92, 4.92, 4.84, 4.65, and 4.51 have C-1s resonating at δ101.57, 95.73, 101.40, 102.56, 100.97, and 103.36, respectively (for a summary, see Table S1 in the supplemental material). The $J_{C,H}$ values for each of these protons were calculated to be 171, 170, 171, 170, 169, and 161 Hz by measurement of the inverse-detection nondecoupled two-dimensional HMQC (Fig. 6). These results established that the terminal amido-Hex was a β configuration and the others were α-anomers.

Cloning and sequence of serotype 16 GPI biosynthesis cluster. To isolate the serotype 16 GPI biosynthesis cluster, the genomic cosmid library of *M. intracellulare* serotype 16 strain ATCC 13950^T was constructed. Primers were designed to amplify the region corresponding to the *rfbA* gene. More than 300 cosmid clones were tested using colony PCR with *rfbA* primers, and the positive clones no. 51 and 253 were isolated from the *E. coli* transductants. PCR analysis revealed that clone no. 253 contained a *dnrC* gene but that clone no. 51 did not. Thus, we used clone no. 253 for subsequent sequence analysis for the *gtfB-dnrC* region. The 22.9-kb region of *M. intracellulare* sero-

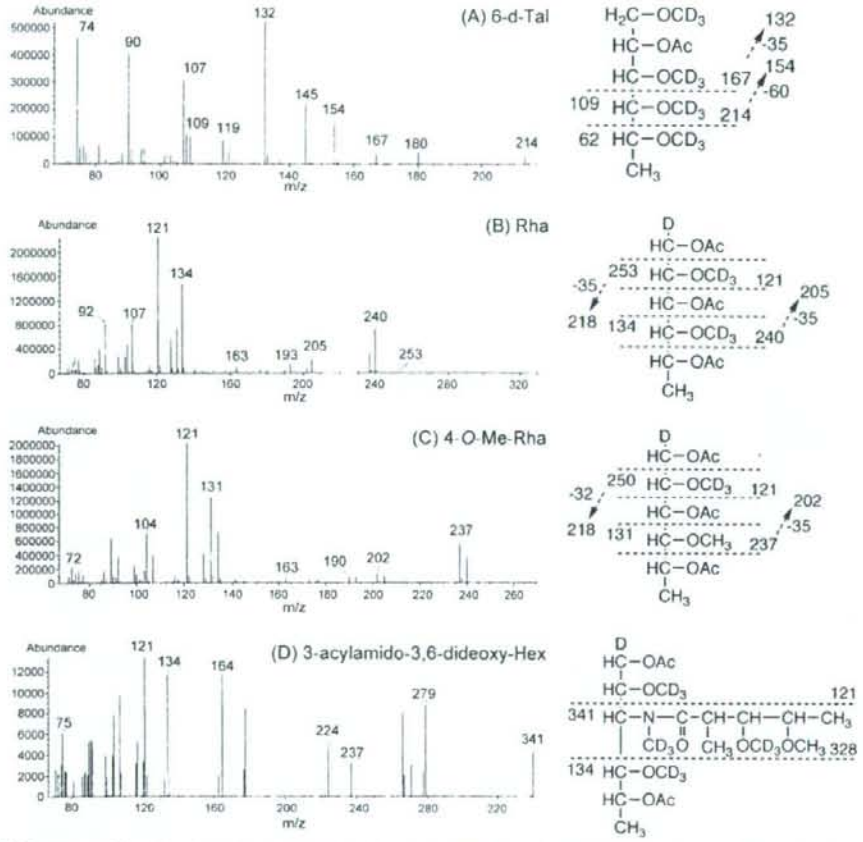

FIG. 4. GC-MS spectra of individual perdeuteromethylated alditol acetate derivatives from serotype 16 OSE. The formation of prominent fragment ions is illustrated; fragments were assigned to 1,3,4,5-tetra-*O*-deuteromethyl-2-*O*-acetyl-6-deoxy-talitol (A), 2,4-di-*O*-deuteromethyl-1,3,5-tri-*O*-acetyl-rhamnitol (B), 2-*O*-deuteromethyl-4-*O*-methyl-1,3,5-tri-*O*-acetyl-rhamnitol (C), and 2,4-di-*O*-deuteromethyl-1,5-di-*O*-acetyl-3-2'-methyl-3'-*O*-deuteromethyl-4'-methoxy-pentanoyl-deuteromethylamido-3,6-dideoxy-hexitol (D).

type 16 ATCC 13950^T was deposited in the NCBI GenBank database (accession no. AB355138). The similarity to protein sequences of each ORF is summarized in Table 1, and the genetic map for the serotype 16 GPI, biosynthetic cluster was compared with those of serotype 2, 4, and 7 GPI s (Fig. 7). The *gtfB* and *drrC* genes of *M. intracellulare* serotype 16 ATCC 13950^T had 99.8% and 83.7% DNA identities with those of *M. intracellulare* serotype 7 ATCC 35847, respectively. In the DNA region between *gtfB* and *drrC* (20.8 kb), 17 ORFs were observed. Four ORFs (ORF 1, 2, 16, and 17) were homologous to those found in the same region of serotype 7-specific DNA, and the others were unique to the serotype 16 strain. No insertion of insertion elements or transposons was detected in this region. The nucleotide sequences of the ORF 1 and ORF 2 in serotype 16 strain ATCC 13950^T were homologous to those of ORF 1 and ORF 8 in serotype 7, respectively, suggesting that these two ORFs have the same function. The similarity of the deduced amino acid sequences suggested the possibility that the functions of ORF 3 and ORF 6 are to encode methyltransferase and aminotransferase, respectively. The deduced amino acid sequences of ORF 4 and ORF 5 showed significant similarities to the WxeM protein, the function of which is not clear. Interestingly, the deduced amino acid sequences of ORF 16 and ORF 17 of serotype 16 were homologous to ORF 9 of serotype 7. ORFs 1, 16, and 17 have considerable homology to glycosyltransferases. Nine ORFs, which are possibly involved in fatty acid synthesis, were detected between ORF 7 and ORF 15. It is notable that ORF 13 had a chimeric structure. The N-terminal half of ORF 13 showed similarity to phosphate butyryl/acetyl transferases, but the C-terminal half showed similarity to short-chain reductase/dehydrogenases. These results suggest that this region of DNA is responsible for the biosynthesis of the serotype 16-specific GPI.

Expression of cosmid clone no. 253 in *M. avium* serotype 1 strain. The OSE of serotype 1 GPI, was composed of α-1-Rha-

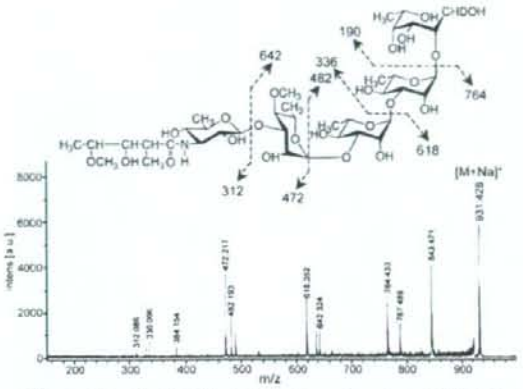

FIG. 5. MALDI-TOF/TOF MS spectrum of serotype 16 OSE. The formation of a characteristic increment in fragment ions is illustrated. The matrix was 10 mg/ml 2,5-dihydroxybenzoic acid in ethanol-water (3:7, vol/vol), and it was performed in the lift-lift mode. Intens., intensity; a.u., absorbance units.

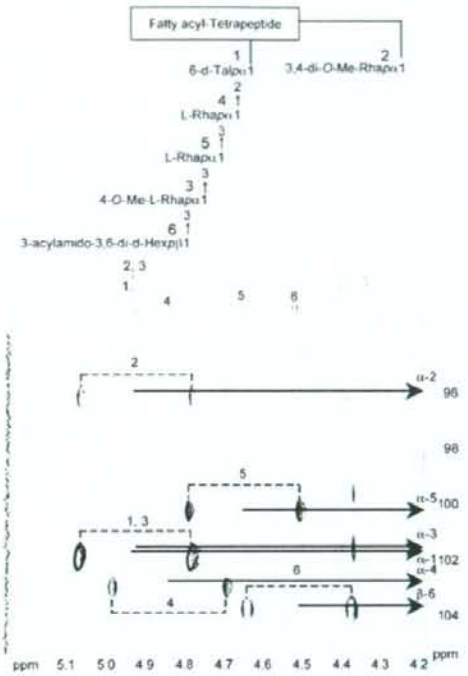

FIG. 6. Nondecoupled ^{1}H-detected [^{1}H, ^{13}C] HMQC spectrum of serotype 16 GPL. Cross-peak labels correspond to those shown on the structure.

(1→2)-6-d-L-Tal (9). The *M. avium* serotype 1 strain (NF113) was transformed with cosmid clone no. 253 containing a serotype 16-specific gene cluster and produced a new GPL with a different R_f value by TLC compared to serotype 1 GPL (Fig. 8A). The R_f value of the new GPL was identical to that of the serotype 16 GPL. The molecular weight of intact GPL, the fragment pattern of its OSE, and the GC pattern of the alditol acetate derivatives were completely equivalent to those of the serotype 16 GPL (see Fig. S2 in the supplemental material). As a result, the transformant of the serotype 1 strain expressed the cosmid clone no. 253 gene cluster and produced the serotype 16 GPL.

DISCUSSION

MAC species have serotype-specific GPLs that are characteristic components of the outer layer of the cell wall (6, 9). In addition to their serological differentiation, the chemical structures of 15 serotype-specific GPLs derived from the predominant clinical isolates have been analyzed; however, those of other GPLs remain unclear. The present study demonstrates the chemical structure of the serotype 16 GPL derived from *M. intracellulare*. We determined the glycosyl composition, linkage positions, and anomeric and ring configurations of the glycosyl residues of the serotype 16 GPL, and its OSE was defined as 3-2′-methyl-3′-hydroxy-4′-methoxy-pentanoyl-amido-3,6-dideoxy-β-Hex-(1→3)-4-*O*-methyl-α-L-Rha-(1→3)-α-L-Rha-(1→3)-α-L-Rha-(1→2)-6-d-α-L-Tal (Fig. 8B). The serotype 16 GPL should be listed as a group 2 polar GPL in the structural classification of Chatterjee and Khoo (9).

The GPLs of serotypes 7, 12, 17, and 19 have already been classified as group 2 GPLs, which are commonly composed of R→α-L-Rha-(1→3)-α-L-Rha-(1→2)-6-d-L-Tal (R, variable region), possessing a characteristic terminal sugar such as *N*-acyldeoxy-Hex. Indeed, the presence of an amido sugar has been reported in only five GPLs, serotypes 7, 12, 14, 17, and 25 (8, 9, 18). It has been determined that the OSE structure of the serotype 17 GPL was 3-2′-methyl-3′-hydroxy-butanoyl-amido-3,6-dideoxy-β-D-Glc-(1→3)-4-*O*-methyl-α-L-Rha-(1→3)-α-L-Rha-(1→3)-α-L-Rha-(1→2)-6-d-L-Tal (9, 25). Based on the behavior of GPLs in TLC and the GC-MS analysis of alditol acetate derivatives, serotype 16 GPL seems to possess a unique carbohydrate epitope similar to that of serotype 17 GPL. We compared the OSE of serotype 16 GPL to that of serotype 17 GPL. The acylated amido group that was bound to the terminal sugar was different, although the linkage position was identical. Except for the terminal-acylated amido sugar, the other sugar compositions and glycosyl linkage positions were completely identical. An acylated amido group attached to the C-3 position of Hex is very unusual. To our knowledge, 3-amido-Hex is irregular in nature, although 2-amido-Hex is known to be glucosamine or galactosamine, which is frequently isolated as a component of lipopolysaccharides and glycosaminoglycans in prokaryotic and eukaryotic cells (7, 42). Further, existence of short-chain fatty acid 2-methyl-3-hydroxy-4-methoxy-pentanoic acid linked to the amido group of d-Hex is also unique. The characteristic gene cluster is thought to regulate the production of 3-acylated-amido-Hex. It is difficult to determine the species of acylated amido sugars, because no reference standard is available. The terminal sugar of the serotype 17 GPL was reviewed as a gluco-configuration, although firm evidence was not shown (9, 25). The $J_{4,11}$ and $J_{1,2}$ values for the anomeric proton in the terminal sugar were 16I and 7.7 Hz,

TABLE 1. Similarity to protein sequences of ORFs in cosmid clone no. 253 derived from *M. intracellulare* serotype 16 strain ATCC 13950[T]

ORF	Predicted molecular mass (kDa)	Predicted pI	Exhibits similarity to	E value	Amino acid identity (no. matched/total no.)	Accession no.
GtfB	45.6	6.35	Glycosyltransferase GtfB	0.0	417/418	BAF45360
Orf 1	45.2	6.10	Putative glycosyltransferase	0.0	416/417	BAF45361
Orf 2	78.9	8.51	Putative acyltransferase	0.0	557/728	BAF45368
Orf 3	31.0	5.88	Putative methyltransferase	2e-89	382/421	NP_218045
Orf 4	15.7	4.94	Conserved hypothetical protein	1e-39	73/129	BAD50406
Orf 5	16.0	4.69	Conserved hypothetical protein	5e-40	75/135	EAX55190
Orf 6	41.1	5.88	Aminotransferase/DegT_DnrJ_EryC1	6e-119	208/357	ABD68440
Orf 7	40.6	9.65	Conserved hypothetical protein	2e-89	178/304	AAS03547
Orf 8	36.7	5.32	Conserved hypothetical protein	2e-52	116/298	CAE06954
Orf 9	22.3	9.79	Putative *N*-acetyltransferase	4e-14	58/166	EAU11841
Orf 10	25.3	7.82	Short-chain dehydrogenase/reductase	7e-47	101/233	EAO61220
Orf 11	23.8	6.05	Putative hydrolase	4e-24	64/196	ABG85599
Orf 12	37.2	6.50	Ketoacyl-acyl carrier protein synthase III	3e-55	126/331	EAX48715
Orf 13	42.5	7.72	Short-chain dehydrogenase/reductase	2e-42	97/248	ZP_01289005
Orf 14	65.8	4.70	Predicted enzyme involved in methoxymalonyl-acyl carrier protein biosynthesis	6e-85	201/575	ABB73590
Orf 15	50.0	6.23	Acyl coenzyme A synthetases	2e-128	233/445	EAI27362
Orf 16	39.1	8.00	Putative glycosyltransferase	2e-106	196/318	NP_855197
Orf 17	37.7	9.46	Putative glycosyltransferase	8e-160	278/323	BAF45369
DrrC	28.6	11.47	Daunorubicin resistance protein C	6e-132	233/261	BAF45370

respectively (Fig. 6; Table S1 in the supplemental material). These results demonstrated unequivocally that the terminal amido-Hex was β configuration and II-2 was in the axial position. The terminal amido-Hex is considered to be derived from glucose or galactose, not Rha.

Next, we explored the genetic mechanism of GPI biosynthesis, because the elongation of carbohydrate chains in serotype-specific GPIs is poorly understood. The *ser2* gene cluster of the *M. avium* serotype 2 strain (31) and a 27.5-kb DNA fragment of the *M. avium* serotype 4 strain (28) were identified to be responsible for the biosynthesis of each OSE in GPIs. Recently, enzymatic characterizations of glycosyltransferase and methyltransferase of nonpolar GPIs have been reported for *Mycobacterium smegmatis* (36, 38). In the serotype-specific polar GPI biosynthesis of MAC, only the *rtfA* gene was functionally clarified to encode the transfer of L-Rha to 6-d-Tal, but which gene cluster transfers the sugars next to L-Rha elongated from 6-d-Tal is unclear.

In this study, we cloned the biosynthetic cluster of the serotype 16 GPI, and analyzed its sequence. Seventeen ORFs were detected in the serotype 16 strain, and the sequence homology was analyzed. The transformant of the *M. avium* serotype 1

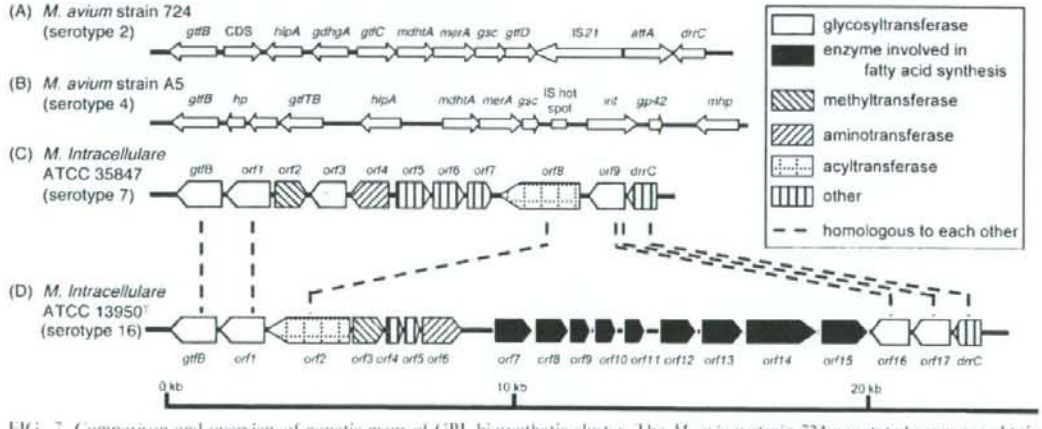

FIG. 7. Comparison and overview of genetic maps of GPI biosynthetic cluster. The *M. avium* strain 724 annotated sequence obtained from GenBank (accession no. AF125999) (A); the *M. avium* strain A5 annotated sequence obtained from GenBank (accession no. AY130970) (B); the *M. intracellulare* ATCC 35847 sequenced in our previous study (GenBank accession no. AB274811) (C); the *M. intracellulare* ATCC 13950[T] sequenced in this study (GenBank accession no. AB355138) (D). The orientation of each gene is shown by the direction of the arrow. In panels A and B, putative ORFs not showing homology to known proteins sequences are not depicted. The sequences extending upstream in panels A and B and downstream in panel B are not included in the figure.

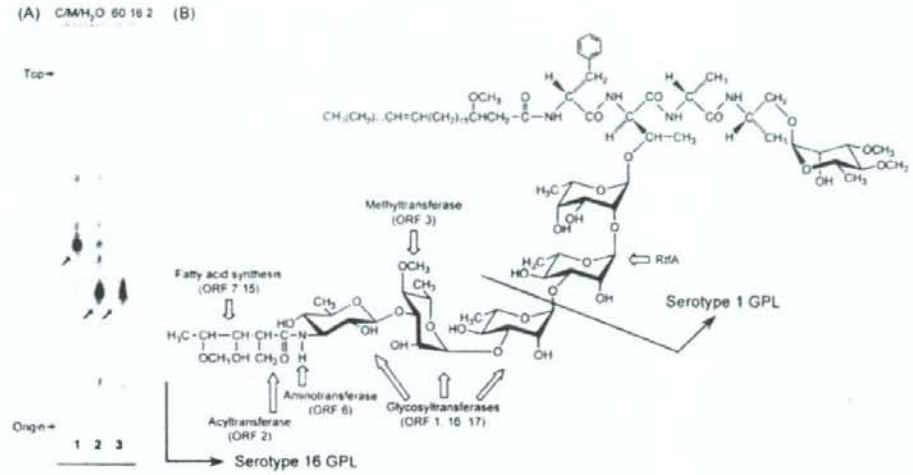

FIG. 8. TLC pattern of *M. avium* serotype 1 and its transformant with cosmid clone no. 253 and proposed complete structure of the serotype 16 GPI. (A) The alkaline-stable lipids derived from *M. avium* serotype 1 (lane 1), its transformant (lane 2), and purified serotype 16 GPI (lane 3) were developed with the solvent system of chloroform-methanol-water (60:16:2, vol/vol/vol). (B) Predicted biosynthesis gene clusters are indicated by arrows.

strain carrying cosmid clone no. 253 produced serotype 16 GPI. These results strongly implied that this *gtfB-dnrC* region is responsible for the biosynthesis of the serotype 16-specific GPI. From the structural analysis of the serotype 16 GPI and the sequence of cosmid clone no. 253, it is possible to predict the relationship between the biosynthesis of serotype 16 GPI and the function of each ORF.

The genetic map of the serotype 16 GPI biosynthetic cluster was compared to those of serotype 2 GPI from *M. avium* strain 724, serotype 4 GPI from *M. avium* strain A5, and serotype 7 GPI from *M. intracellulare* strain ATCC 35847[T] (12, 18, 28). Significant differences were found in the neighborhood of the conserved region. The genetic organization of the serotype 16 GPI gene cluster was distinct from that of serotype 7, except for some of the ORFs, and the ORFs in this region of serotype 2 and serotype 4 were completely different from ORFs 1 to 17 in serotype 16 (Fig. 7).

In addition to *M. intracellulare* serotype 7 (18) and serotype 16 strains, we have analyzed similar gene clusters of *M. intracellulare* serotype 12 and 17 strains. The sequence homology of the regions of ORF 1 and ORF 17 was highly conserved between only *M. intracellulare* serotype 16 and 17 strains (unpublished data). ORFs 1, 16, and 17 may lead to transfer of the two additional molecules of L-Rha and terminal amido-Hex. ORF 2 was assigned to acyltransferase and may be responsible for biosynthesis of the 3-2'-methyl-3'-hydroxy-4'-methoxy-pentanoyl-amido group in the terminal Hex. ORF 3 is probably responsible for the transfer of the *O*-methyl group at the C-4 position in the third L-Rha from 6-d-Tal. ORF 6 is homologous to aminotransferase and possibly associated with the biosynthesis of an amido group in the terminal Hex. The deduced amino acid sequences of ORF 6 in serotype 16 and ORF 4 in serotype 7 have homologies to DegT_DnrJ_EryC1 aminotransferases. However, these two ORFs are dissimilar to each other. Serotype 16 and 7 GPLs have an amido group at the terminal Hex, although the attachment position is different. The serotype 7 GPL has an amido group at the C-4 position in the terminal Hex, but the serotype 16 GPL has it at the C-3 position. Nine ORFs between ORF 7 and ORF 15 are possibly involved in fatty acid synthesis of the acyl chain moiety linked by an amido bond of the terminal Hex. Taken together, this gene cluster may participate in the biosynthetic pathway of the serotype 16-specific GPL, although further study is needed to clarify the function of each ORF.

Recent studies suggest that GPLs play an important role in the phenotype and pathogenicity of MAC. The colony morphology is considered to be influenced by cell wall GPL. MAC colony phenotypes spontaneously occur from smooth to rough type, and this is due to a mutation lacking GPL (3, 13, 22). The deletion of genomic regions encoding GPL biosynthesis may result in the loss of GPL. Danelishvili et al. demonstrated that the uptake by and growth in macrophages of a MAC mutant with the gene belonging to the GPL synthesis pathway inactivated by transposon insertion were decreased (11). Bhatnagar and Schorey have reported that macrophages infected with MAC release exosomes containing GPLs that result in the transfer of the GPLs to uninfected macrophages and induce a proinflammatory response (4). These findings imply that GPL participates in the pathogenicity of MAC. By contrast, our previous studies have demonstrated that anti-GPL antibodies are detected in the sera of most immunocompetent patients with MAC pulmonary disease and that the detection of anti-GPL antibody is useful for the serodiagnosis of MAC disease (15, 26, 27).

To understand the role of GPLs in MAC and its hosts, it is necessary to define the chemical structure and biosynthesis pathways of GPLs. Elucidation of the structure-function relationship of GPL may open a new avenue for controlling MAC disease.

ACKNOWLEDGMENTS

This work was supported by grants from the Ministry of Education, Culture, Sports, Science, and Technology of Japan, the Japan Health Sciences Foundation, and the Ministry of Health, Labor, and Welfare of Japan (Research on Emerging and Reemerging Infectious Diseases).

We are grateful to Sumihiro Hase (Department of Chemistry, Graduate School of Science, Osaka University, Osaka, Japan) and Hiromi Murakami (Osaka Municipal Technical Research Institute, Osaka, Japan) for helpful discussion.

REFERENCES

1. **Baess, I.** 1983. Deoxyribonucleic acid relationships between different serovars of *Mycobacterium avium*, *Mycobacterium intracellulare* and *Mycobacterium scrofulaceum*. Acta Pathol. Microbiol. Immunol. Scand. **91:**201–203.
2. **Barrow, W. W., T. L. Davis, E. L. Wright, V. Labrousse, M. Bachelet, and N. Rastogi.** 1995. Immunomodulatory spectrum of lipids associated with *Mycobacterium avium* serovar 8. Infect. Immun. **63:**126–133.
3. **Belisle, J. T., K. Klaczkiewicz, P. J. Brennan, W. R. Jacobs, Jr., and J. M. Inamine.** 1993. Rough morphological variants of *Mycobacterium avium*. Characterization of genomic deletions resulting in the loss of glycopeptidolipid expression. J. Biol. Chem. **268:**10517–10523.
4. **Bhatnagar, S., and J. S. Schorey.** 2007. Exosomes released from infected macrophages contain *Mycobacterium avium* glycopeptidolipids and are proinflammatory. J. Biol. Chem. **282:**25779–25789.
5. **Bhatt, A., N. Fujiwara, K. Bhatt, S. S. Gurcha, L. Kremer, B. Chen, J. Chan, S. A. Porcelli, K. Kobayashi, G. S. Besra, and W. R. Jacobs, Jr.** 2007. Deletion of *kasB* in *Mycobacterium tuberculosis* causes loss of acid-fastness and subclinical latent tuberculosis in immunocompetent mice. Proc. Natl. Acad. Sci. USA **104:**5157–5162.
6. **Brennan, P. J., and H. Nikaido.** 1995. The envelope of mycobacteria. Annu. Rev. Biochem. **64:**29–63.
7. **Campo, G. M., S. Campo, A. M. Ferlazzo, R. Vinci, and A. Calatroni.** 2001. Improved high-performance liquid chromatographic method to estimate aminosugars and its application to glycosaminoglycan determination in plasma and serum. J. Chromatogr. B **765:**151–160.
8. **Chatterjee, D., G. O. Aspinall, and P. J. Brennan.** 1987. The presence of novel glucuronic acid-containing, type-specific glycolipid antigens within *Mycobacterium* spp. Revision of earlier structures. J. Biol. Chem. **262:**3528–3533.
9. **Chatterjee, D., and K. H. Khoo.** 2001. The surface glycopeptidolipids of mycobacteria: structures and biological properties. Cell. Mol. Life Sci. **58:** 2018–2042.
10. **Daffe, M., and P. Draper.** 1998. The envelope layers of mycobacteria with reference to their pathogenicity. Adv. Microb. Physiol. **39:**131–203.
11. **Danelishvili, L., M. Wu, B. Stang, M. Harriff, S. Cirillo, J. Cirillo, R. Bildfell, B. Arbogast, and L. E. Bermudez.** 2007. Identification of *Mycobacterium avium* pathogenicity island important for macrophage and amoeba infection. Proc. Natl. Acad. Sci. USA **104:**11038–11043.
12. **Eckstein, T. M., J. T. Belisle, and J. M. Inamine.** 2003. Proposed pathway for the biosynthesis of serovar-specific glycopeptidolipids in *Mycobacterium avium* serovar 2. Microbiology **149:**2797–2807.
13. **Eckstein, T. M., J. M. Inamine, M. L. Lambert, and J. T. Belisle.** 2000. A genetic mechanism for deletion of the *ser2* gene cluster and formation of rough morphological variants of *Mycobacterium avium*. J. Bacteriol. **182:** 6177–6182.
14. **Eckstein, T. M., F. S. Silhaq, D. Chatterjee, N. J. Kelly, P. J. Brennan, and J. T. Belisle.** 1998. Identification and recombinant expression of a *Mycobacterium avium* rhamnosyltransferase gene (*rtfA*) involved in glycopeptidolipid biosynthesis. J. Bacteriol. **180:**5567–5573.
15. **Enomoto, K., S. Oka, N. Fujiwara, T. Okamoto, Y. Okuda, R. Maekura, T. Kuroki, and I. Yano.** 1998. Rapid serodiagnosis of *Mycobacterium avium-intracellulare* complex infection by PHSA with cord factor (trehalose 6, 6′-dimycolate), and serotyping using the glycopeptidolipid antigen. Microbiol. Immunol. **42:**689–696.
16. **Falkinham, J. O., III.** 1996. Epidemiology of infection by nontuberculous mycobacteria. Clin. Microbiol. Rev. **9:**177–215.
17. **Field, S. K., D. Fisher, and R. L. Cowie.** 2004. *Mycobacterium avium* complex pulmonary disease in patients without HIV infection. Chest **126:**566–581.
18. **Fujiwara, N., N. Nakata, S. Maeda, T. Naka, M. Doe, I. Yano, and K. Kobayashi.** 2007. Structural characterization of a specific glycopeptidolipid containing a novel *N*-acyl-deoxy sugar from *Mycobacterium intracellulare* serotype 7 and genetic analysis of its glycosylation pathway. J. Bacteriol. **189:**1099–1108.
19. **Gerwig, G. J., J. P. Kamerling, and J. F. G. Vliegenthart.** 1978. Determination of the D and L configuration of neutral monosaccharides by high-resolution capillary G.L.C. Carbohydr. Res. **62:**349–357.
20. **Hakomori, S.** 1964. A rapid permethylation of glycolipid, and polysaccharide catalyzed by methylsulfinyl carbanion in dimethyl sulfoxide. J. Biochem. (Tokyo) **55:**205–208.
21. **Heidelberg, T., and O. R. Martin.** 2004. Synthesis of the glycopeptidolipid of *Mycobacterium avium* serovar 4: first example of a fully synthetic C-mycoside GPL. J. Org. Chem. **69:**2296–2301.
22. **Howard, S. T., F. Rhoades, J. Recht, X. Pang, A. Alsup, R. Kolter, C. R. Lyons, and T. F. Byrd.** 2006. Spontaneous reversion of *Mycobacterium abscessus* from a smooth to a rough morphotype is associated with reduced expression of glycopeptidolipid and reacquisition of an invasive phenotype. Microbiology **152:**1581–1590.
23. **Kaufmann, S. H.** 2001. How can immunology contribute to the control of tuberculosis? Nat. Rev. Immunol. **1:**20–30.
24. **Khoo, K. H., D. Chatterjee, A. Dell, H. R. Morris, P. J. Brennan, and P. Draper.** 1996. Novel *O*-methylated terminal glucuronic acid characterizes the polar glycopeptidolipids of *Mycobacterium habana* strain TMC 5135. J. Biol. Chem. **271:**12333–12342.
25. **Khoo, K. H., E. Jarhoe, A. Barker, J. Torrelles, C. W. Kuo, and D. Chatterjee.** 1999. Altered expression profile of the surface glycopeptidolipids in drug-resistant clinical isolates of *Mycobacterium avium* complex. J. Biol. Chem. **274:**9778–9785.
26. **Kitada, S., R. Maekura, N. Toyoshima, N. Fujiwara, I. Yano, T. Ogura, M. Ito, and K. Kobayashi.** 2002. Serodiagnosis of pulmonary disease due to *Mycobacterium avium* complex with an enzyme immunoassay that uses a mixture of glycopeptidolipid antigens. Clin. Infect. Dis. **35:**1328–1335.
27. **Kitada, S., Y. Nishiuchi, T. Hiraga, N. Naka, H. Hashimoto, K. Yoshimura, K. Miki, M. Miki, M. Motone, T. Fujikawa, K. Kobayashi, I. Yano, and R. Maekura.** 2007. Serological test and chest computed tomography findings in patients with *Mycobacterium avium* complex lung disease. Eur. Respir. J. **29:**1217–1223.
28. **Krzywinska, E., and J. S. Schorey.** 2003. Characterization of genetic differences between *Mycobacterium avium* subsp. avium strains of diverse virulence with a focus on the glycopeptidolipid biosynthesis cluster. Vet. Microbiol. **91:**249–264.
29. **Maekura, R., Y. Okuda, A. Hirotani, S. Kitada, T. Hiraga, K. Yoshimura, I. Yano, K. Kobayashi, and M. Ito.** 2005. Clinical and prognostic importance of serotyping *Mycobacterium avium-Mycobacterium intracellulare* complex isolates in human immunodeficiency virus-negative patients. J. Clin. Microbiol. **43:**3150–3158.
30. **Marras, T. K., and C. L. Daley.** 2002. Epidemiology of human pulmonary infection with nontuberculous mycobacteria. Clin. Chest Med. **23:**553–567.
31. **Maslow, J. N., V. R. Irani, S. H. Lee, T. M. Eckstein, J. M. Inamine, and J. T. Belisle.** 2003. Biosynthetic specificity of the rhamnosyltransferase gene of *Mycobacterium avium* serovar 2 as determined by allelic exchange mutagenesis. Microbiology **149:**3193–3202.
32. **McClatchy, J. K.** 1981. The seroagglutination test in the study of nontuberculous mycobacteria. Rev. Infect. Dis. **3:**867–870.
33. **McCloskey, J. A.** 1969. Mass spectrometry, p. 402. *In* J. M. Lowenstein (ed.), Methods in enzymology: lipid, vol. 14. Academic Press, New York, NY.
34. **McNeil, M., H. Gaylord, and P. J. Brennan.** 1988. *N*-formylkansosaminyl-(1-3)-2-*O*-methyl-D-rhamnopyranose: the type-specific determinant of serovariant 14 of the *Mycobacterium avium* complex. Carbohydr. Res. **177:**185–198.
35. **McNeil, M., A. Y. Tsang, and P. J. Brennan.** 1987. Structure and antigenicity of the specific oligosaccharide hapten from the glycopeptidolipid antigen of *Mycobacterium avium* serotype 4, the dominant *Mycobacterium* isolated from patients with acquired immune deficiency syndrome. J. Biol. Chem. **262:** 2630–2635.
36. **Miyamoto, Y., T. Mukai, N. Nakata, Y. Maeda, M. Kai, T. Naka, I. Yano, and M. Makino.** 2006. Identification and characterization of the genes involved in glycosylation pathways of mycobacterial glycopeptidolipid biosynthesis. J. Bacteriol. **188:**86–95.
37. **Odham, G., and E. Stenhagen.** 1972. Fatty acids, p. 211–228. *In* G. R. Waller (ed.), Biochemical application of mass spectrometry. Wiley-Interscience, New York, NY.
38. **Patterson, J. H., M. J. McConville, R. F. Haites, R. L. Coppel, and H. Billman-Jacobe.** 2000. Identification of a methyltransferase from *Mycobacterium smegmatis* involved in glycopeptidolipid synthesis. J. Biol. Chem. **275:**24900–24906.
39. **Supply, P., E. Mazars, S. Lesjean, V. Vincent, B. Gicquel, and C. Locht.** 2000. Variable human minisatellite-like regions in the *Mycobacterium tuberculosis* genome. Mol. Microbiol. **36:**762–771.
40. **Tsang, A. Y., J. C. Denner, P. J. Brennan, and J. K. McClatchy.** 1992. Clinical and epidemiological importance of typing of *Mycobacterium avium* complex isolates. J. Clin. Microbiol. **30:**479–484.
41. **Wayne, L. G., and H. A. Sramek.** 1992. Agents of newly recognized or infrequently encountered mycobacterial diseases. Clin. Microbiol. Rev. **5:**1–25.
42. **Woods, A., and J. R. Conchman.** 2001. Proteoglycan isolation and analysis, p. 10.7.1–10.7.19. *In* J. S. Bonifacino, M. Dasso, J. B. Harford, J. Lippincott-Schwartz, and K. M. Yamada (ed.), Current protocols in cell biology. Wiley Interscience, Hoboken, NJ.

Microbial Pathogenesis 46 (2009) 6–12

Contents lists available at ScienceDirect

Microbial Pathogenesis

journal homepage: www.elsevier.com/locate/micpath

Virulence of *Mycobacterium avium* complex strains isolated from immunocompetent patients

Yoshitaka Tateishi [a,b,*], Yukio Hirayama [a], Yuriko Ozeki [a,c], Yukiko Nishiuchi [a,d], Mamiko Yoshimura [a], Jing Kang [a], Atsushi Shibata [a], Kazuto Hirata [e], Seigo Kitada [b], Ryoji Maekura [b], Hisashi Ogura [f], Kazuo Kobayashi [g], Sohkichi Matsumoto [a,*]

[a] Department of Bacteriology, Osaka City University Graduate School of Medicine, 1-4-3 Asahi-machi, Abeno-ku, Osaka 545-8585, Japan
[b] Department of Internal Medicine, National Hospital Organization Toneyama National Hospital, 5-1-1 Toneyama, Toyonaka, Osaka 560-8552, Japan
[c] Sonoda Women's University, 7-29-1 Minamitsukaguchi-cho, Amagasaki, Hyogo 661-8520, Japan
[d] Toneyama Institute for Tuberculosis Research, Osaka City University Medical School, Toyonaka 5-1-1, Toneyama, Toyonaka, Osaka 560-8552, Japan
[e] Department of Respiratory Medicine, Osaka City University Graduate School of Medicine, 1-4-3 Asahi-machi, Abeno-ku, Osaka 545-8585, Japan
[f] Department of Virology, Osaka City University Graduate School of Medicine, 1-4-3 Asahi-machi, Abeno-ku, Osaka 545-8585, Japan
[g] Department of Immunology, National Institute of Infectious Diseases, 1-23-1, Toyama, Shinjuku-ku, Tokyo 162-8640, Japan

ARTICLE INFO

Article history:
Received 6 August 2008
Received in revised form
29 September 2008
Accepted 2 October 2008
Available online 1 November 2008

Keywords:
Mycobacterium avium complex
Virulence
Clinical isolates
Immunocompetent humans
Pulmonary disease

ABSTRACT

Mycobacterium avium complex (MAC) disease has been increasing worldwide not only in immunocompromised but also in immunocompetent humans. However, the relationship between mycobacterial strain virulence and disease progression in immunocompetent humans is unclear. In this study, we isolated 6 strains from patients with pulmonary MAC disease. To explore the virulence, we examined the growth in human THP-1 macrophages and pathogenicity in C57BL/6 mice. We found that one strain, designated 198, which was isolated from a patient showing the most progressive disease, persisted in THP-1 cells. In addition, strain 198 grew to a high bacterial load with strong inflammation in mouse lungs and spleens 16 weeks after infection. To our knowledge, strain 198 is the first isolated MAC strain that exhibits hypervirulence consistently for the human patient, human macrophages *in vitro*, and even for immunocompetent mice. Other strains showed limited survival and weak virulence both in macrophages and in mice, uncorrelated to disease progression in human patients. We demonstrated that there is a hypervirulent clinical MAC strain whose experimental virulence corresponds to the serious disease progression in the patients. The existence of such strain suggests the involvement of bacterial virulence in the pathogenesis of pulmonary MAC disease in immunocompetent status.

1. Introduction

Mycobacterium avium complex (MAC) is the most common cause of human infection due to nontuberculous mycobacteria. Initially MAC was regarded as only an opportunistic pathogen, primarily in acquired immunodeficiency syndrome (AIDS) patients [1]; however, it has now been shown to cause progressive pulmonary disease even in immunocompetent humans [2]. The American Thoracic Society indicates a wide range of clinical manifestation in patients with non-AIDS MAC disease; some patients keep a stable condition for years, whereas others progress their illness rapidly [3]. Furthermore, MAC infection can be more difficult to treat than *M. tuberculosis* due to even fewer available anti-microbial agents [3].

The pathogenesis of MAC infection has been recently investigated with respect to the host immune response. Interferon-gamma (IFN-γ) activates macrophages to produce proteolytic enzymes and other metabolites, which exhibit mycobactericidal effects. Tumor necrosis factor-alpha (TNF-α), of which production is also stimulated by IFN-γ, augments the bactericidal capacity of macrophages and plays a key role in the induction of the acquired immune response against mycobacteria [4]. A defective IFN-γ response has been shown recently to cause disseminated MAC disease in IFN-γ knock out mice and in humans with genetic mutations of IFN-γ receptor [5,6] or autoantibodies to IFN-γ in some young non-AIDS patients [7,8]. In addition to that, the activity of interleukin-10 (IL-10), which is known to inhibit cytokine synthesis by IFN-γ-producing type1 helper T cells (Th1 cells), has been shown to increase susceptibility to MAC infection in immunocompetent mice [9].

* Corresponding authors. Department of Bacteriology, Osaka City University, Graduate School of Medicine, 1-4-3 Asahi-machi, Abeno-ku, Osaka 545-8585, Japan. Tel.: +81 6 6645 3746; fax: +81 6 6645 3747.
E-mail address: y-tateishi@med.osaka-cu.ac.jp (Y. Tateishi).

0882-4010/$ – see front matter © 2008 Elsevier Ltd. All rights reserved.
doi:10.1016/j.micpath.2008.10.007

Besides genetic factors of the host, bacterial virulence should play an important role for the development of MAC disease. While isolates of *M. tuberculosis* are genetically homogeneous at the nucleotide level [10], MAC has high genetic diversity, including the presence of multiple plasmids [11], and thus likely to have a large corresponding diversity in virulence. In the most complete study examining virulence, forty-one MAC isolates from the environment as well as infected humans and animals were compared for virulence in C57BL/6 mice by intravenous injection [12]. Monitoring of the virulence by CFU counts in lungs, livers, and spleens over 4 months revealed three virulence phenotypes; high (logarithmically increasing load), intermediate (chronic infection at a constant load), and low (initial load increase followed by a decrease until clearance). In addition, clinical studies have suggested severe disease outcome in patients infected with some specific strain type of MAC. For example, MAC serovars 1, 4, and 8 *Mycobacterium avium* are associated with disease severity in AIDS patients [13], and a serovar 4 *M. avium* isolate from an AIDS patient was more invasive and proliferative in blood mononuclear cell-derived human macrophages than a serovar 2 strain from chickens [14]. In non-AIDS MAC disease, *Mycobacterium intracellulare* is associated with greater disease progression [15], and moreover, our previous prospective study on 68 non-AIDS patients suggests that serovar 4 *M. avium* is linked to greater disease progression with a pulmonary MAC infection [16]. Taking these previous data into consideration, we hypothesize that relatively hypervirulent MAC strains exist and may be associated with serious disease progression in immunocompetent patients. In order to elucidate the involvement of mycobacterial virulence in the pathogenesis of human pulmonary MAC disease, in this study we examined the difference of mycobacterial virulence of clinical isolates from patients with different disease types using human macrophages and immunocompetent mice.

2. Results

2.1. Characteristics of mycobacterial strains

Six clinical isolates of MAC were isolated from sputum of non-AIDS patients with pulmonary MAC disease, and designated 27, 33, 36, 198, 288, and 347 (Table 1). Strains 33, 198 and 288 were derived from patients with progressive disease against combination chemotherapy recommended by the American Thoracic Society guideline (progressive type) [3]. The patients with progressive disease exhibited higher levels of erythrocyte sedimentation rate (ESR), diffuse and severe pulmonary lesions in chest X-ray findings, and numerous bacteria in the sputum. The patient infected with strain 198 exhibited the most serious disease outcome among study patients in that a right pneumonectomy was needed to prevent disease progression. Strains 27, 36, and 347 were derived from patients with little progression of disease without chemotherapy (silent type). They exhibited lower levels of ESR, segmental pulmonary lesions in chest X-ray findings, and fewer bacteria in the sputum. The isolates belonging to the progressive type consisted of *M. intracellulare* unclassified serovar similar to serovar 12 (strain 198) and *M. avium* apolar type (strains 33 and 288). The isolates belonging to the silent type consisted of *M. intracellulare* serovar 1 (strain 27) and *M. avium* apolar type (strains 36 and 347). For comparison, we employed 2 veterinary strains of *M. avium* ATCC 25291 (serovar 2) as a highly virulent strain in mice [12] and ATCC 35767 (serovar 4) as a low virulent strain. Four clinical isolates other than strains 33 and 347, and ATCC 25291 formed the transparent colony morphology. Strain 33 produced both transparent and rough colony morphologies. Strain 347 and ATCC 35767 displayed smooth opaque colony morphology.

2.2. Growth of clinical isolates in 7H9 broth

All strains showed logarithmic growth from 3 days after culture in 7H9 broth (Table 2). At day 5, two isolates from progressive type (strains 198 and 288) and one isolate from silent type (strain 36) grew significantly slower than ATCC 25291 ($P < 0.005$), and all clinical strains grew significantly slower than ATCC 35767 ($P < 0.0001$). The growth of strain 198 at day 5 was significantly slower than that of strain 27 ($P = 0.001$), and was not significantly different from that of other clinical isolates.

2.3. Virulence of clinical isolates in THP-1 monocyte-derived macrophages

We next studied intracellular survival of the isolates. THP-1 cells, a human monocytic cell line, were differentiated into macrophages by treatment with phorbol 12-myristate 13-acetate (PMA) and infected with MAC strains. Strain 198 grew in THP-1 cells significantly higher than any other strains during 7 days of infection ($P < 0.0001$) (Table 3). Strain 198 grew to approximately 20-fold during 2 days of infection ($P = 0.005$), and even at day 7, it kept the same level of bacterial load as day 0. Strain 36 also grew to approximately 2-fold during 2 days of infection ($P = 0.008$); however, it was rapidly eliminated at day 7, similar to the other strains except for strain 198. There was no significant difference in

Table 1
Characteristics of isolated strains and clinical findings.

Isolates	Species and serovar	Age	Sex	Duration of illness (years)	Erythrocyte sedimentation rate (mm/h)	Chest X-ray findings[a]	Sputum[b]	
							Smear	Culture
Progressive type								
33	*M. avium* apolar type	58	M	17	62	Advanced	2+	3+
198	*M. intracellulare* unclassified serovar[c]	62	F	3	108	Advanced	2+	2+
288	*M. avium* apolar type	56	F	12	78	Advanced	2+	2+
Silent type								
27	*M. intracellulare* serovar 1	67	F	17	50	Moderate	–	1+
36	*M. avium* apolar type	54	F	9	29	Moderate	–	1+
347	*M. avium* apolar type	79	F	14	50	Moderate	1+	1+

Data and sputum samples were collected at the enrollment of the study in 2003.

[a] Advanced chest X-ray findings were defined as bilateral cavities, giant cavities, or bilateral bronchiectasis, and moderate findings were defined as focal inflammation, small or fewer cavities, or mild bronchiectasis.

[b] Smear findings of sputum were defined as follows in high performance fields of microscopy; –: no bacteria in all fields, 1+: less than one bacteria in several fields, 2+: approximately 1–12 bacteria in one field. Culture findings were defined as follows using Ogawa egg agar; 1+: colonies less than 200, 2+: colonies more than 200 and less than 500, 3+: colonies more than 500 and less than 2000.

[c] The serovar of strain 198 was identified as a new type similar to serovar 12 determined by the liquid chromatography/mass spectrometry.

Table 2
Growth rate of MAC in 7H9 broth.

Strain	Ratio of CFUs at[a]		
	Day 1	Day 3	Day 5
33	0.91 ± 0.28	38 ± 0.86	63 ± 10
198	0.93 ± 0.17	12 ± 1.9	18 ± 4.0
288	0.85 ± 0.20	4.3 ± 1.9	16 ± 0.95
27	1.1 ± 0.25	7.3 ± 2.2	120 ± 21
36	0.83 ± 0.093	5.4 ± 0.21	11.0 ± 1.7
347	0.96 ± 0.16	2.7 ± 1.1	44 ± 19
25291	1.6 ± 0.25	4.8 ± 0.24	110 ± 16*
35767	0.97 ± 0.12	11 ± 3.0	370 ± 43**

* Significantly different ($P < 0.005$) from values for strain 198, 288, and 36 as calculated by Scheffé's test.
** Significantly different ($P < 0.0001$) from values for all clinical strains as calculated by Scheffé's test.
[a] Means ± standard deviations of the ratio of CFUs to those at day 0.

the growth rate among these strains except strain 198 during infection.

On light microscopic observation, THP-1 cell morphologies were not different between infected and uninfected cells (data not shown). We then assessed cytotoxicity by the levels of lactate dehydrogenase (LDH) released into the culture supernatants at day 7. The LDH release was detectable in strain 33 and the laboratory strains (strain 33; 5.8 ± 1.5%, ATCC 25291; 11 ± 1.0%, ATCC 35767; 12 ± 1.9%, without significant difference among these strains); however, it was not detectable in other clinical isolates.

2.4. Pathogenesis of clinical isolates in mice

Female C57BL/6 mice were infected by intratracheal instillation with each strain. Bacterial load in lungs, livers, and spleens were evaluated, and histological inflammation was visually analyzed in 5-mice per strain at defined time points during 16 weeks of infection. There was no significant difference in lung CFUs among strains tested 1 day after the inoculation.

Strain 198 showed high bacterial load, and tended to increase gradually both in lungs and spleens during 16 weeks of infection ($P = 0.08$ between day 1 and 16 weeks) (Fig. 1). Strain 198 was loaded in lungs significantly higher than strain 27 ($P = 0.04$) and 33 ($P = 0.0006$) at 8 weeks of infection, and than strain 33 ($P = 0.0009$), 288 ($P = 0.001$), 36 ($P = 0.0003$), and 347 ($P = 0.004$) at 16 weeks. Histologically, strain 198 induced strong inflammation in lungs, which was paralleled with bacterial loads (Fig. 2). ATCC 25291, known as highly a virulent strain in mice [12], showed initial reduction of bacterial load in lungs at 4 weeks of infection ($P = 0.01$ between day 1 and 4 weeks) and rapid increase in bacterial load in lungs after 4 weeks of infection. ATCC 25291 was comparatively virulent to strain 198 with respect to the high bacterial load in lungs and spleens, and severe pulmonary inflammation at 16 weeks of infection. By contrast, other clinical isolates did not increase profoundly in lung CFUs; however, these strains were never eliminated from lungs. ATCC 35767 was rapidly decreased and undetectable in lungs, spleens and livers within 16 weeks of infection. Overall, the clinical isolates other than strain 198 exhibited limited histological lesions with transient inflammatory changes in lungs 4 weeks after the inoculation, and thereafter the inflammation subsided at 16 weeks.

Table 3
Growth rate of MAC in THP-1 cells.

strain	Ratio of CFUs at[a]	
	Day 2	Day 7
33	0.29 ± 0.12	0.25 ± 0.16
198	18 ± 12*	1.30 ± 0.68*
288	0.47 ± 0.26	0.097 ± 0.055
27	0.54 ± 0.37	0.28 ± 0.11
36	2.4 ± 1.2	0.31 ± 0.11
347	1.1 ± 0.49	0.36 ± 0.23
25291	0.16 ± 0.048	0.11 ± 0.038
35767	0.059 ± 0.029	0.0070 ± 0.0048

* Significantly different ($P < 0.0001$) from values for any other strains studied as calculated by Scheffé's test.
[a] Means ± standard deviations of the ratio of CFUs to those at day 0.

3. Discussion

Virulence is defined as the quantitative ability of an agent to cause disease. The virulence of mycobacteria can be evaluated by the infection to macrophages and animals [17]. This is the first study that examined the virulence of MAC isolates from immunocompetent patients with different types of disease outcome. We found that strain 198, which derived from a patient with most serious disease, revealed high bacterial load both in THP-1 cells and in C57BL/6 mice among isolates studied. Strain-specific virulence of MAC has been implicated by some previous studies of the serovar 4 *M. avium* isolated from patients. In AIDS-related MAC disease, a serovar 4 *M. avium* isolate has shown to be one of the frequently isolated type [13], and a previous analysis of a serovar 4 isolate and ATCC strain has shown the superior virulence of serovar 4 *M. avium* in human macrophages [14]. In non-AIDS pulmonary MAC disease, our recent prospective study indicates that patients infected with serovar 4 *M. avium* has poorer prognosis than those infected with MAC of other serovars [16]; however, to our best knowledge, no study has shown the direct data of mycobacterial virulence of clinical isolates and clinical disease outcome. Strain 198 is the first MAC isolate whose experimental virulence corresponds to the serious disease outcome in humans. Thus, strain 198 has strain-specific strong virulence for immunocompetent humans and mice. We consider that strain 198 is worth further genetic investigation of virulence factors.

MAC strains hypervirulent for mice has been isolated previously by Pedrosa et al. including ATCC 25291 and MAC 101, which proliferate profoundly in mouse macrophages and in mice *in vivo* [12]. In this study, strain 198 proliferated in human macrophages, in correspondence with rapid clinical disease progression and additionally in mouse lungs. The consistency between experimental virulence in human cells and clinical disease outcome suggests that the capability of inducing such strong pathogenesis may be attributed mostly to the characteristics of the pathogen, i.e. virulence factor(s) for mammalian cells unique to strain 198. Previously Birkness et al. has shown the strong cytotoxic effect and growth of serovar 4 *M. avium* isolated from an AIDS patient in blood mononuclear cell-derived human macrophages compared with a serovar 2 strain from chickens (ATCC 35713). Therefore, we evaluated cytotoxicity of MAC strains by the microscopic morphology and by the LDH release from infected THP-1 cells; however, contrary to the expectation, strain 198 was not cytotoxic to THP-1. In addition, the release of LDH was lower in strain 33, ATCC 25291, and ATCC 35767 than in the previous experiment of *M. tuberculosis* infection to THP-1 cells (cytotoxicity in cases of *M. tuberculosis* H37Rv and H37Ra; approximately 30%) [18]. We assume that cytotoxic effect may not play a major role in displaying the virulence of MAC during infection, suggested by the similar result by Huttunen et al. showing the lack of cytotoxic effect of MAC in human 28SC macrophage and A549 lung epithelial cell lines evaluated by 3-(4,5-dimethyl-2-thiazolyl)-2,5-diphenyl-2H tetrazolium bromide (MTT) assay [19]. We speculate the virulence of strain 198 depends on the ability to survive or proliferate in macrophages rather than cytotoxic effect, which, may be causative for severe pulmonary MAC disease with rapid disease progression within a few years.

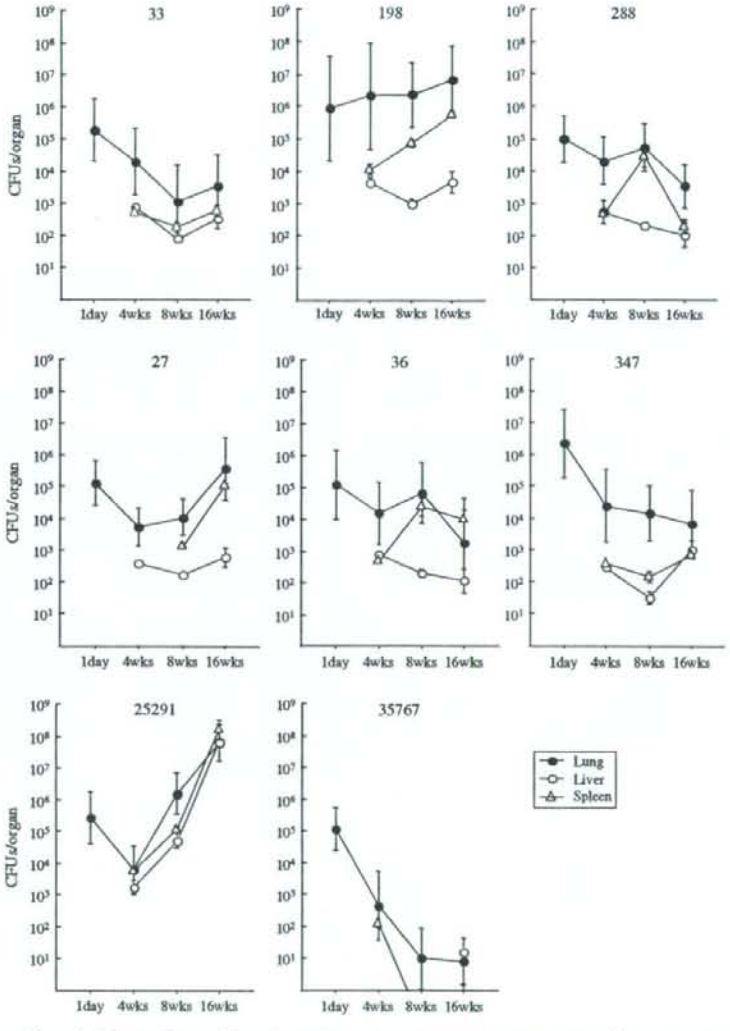

Fig. 1. Time course of mycobacterial growth in lungs, spleens and livers of C57BL/6 mice. Bacterial suspensions containing 1×10^5 CFUs were inoculated intratracheally to female C57BL/6 mice at the age of 7 weeks ($n = 20$ per strain). The lungs, livers and spleens of 5 mice per strain were sectioned at day 1 (only lungs), 4, 8, and 16 weeks later from challenge. Data were presented as means ± standard deviations of CFUs/organ.

In this study, strain 198 showed strong virulence for mice at 16 weeks of infection similar to ATCC 25291; however, virulence for THP-1 cells was quite different, and pathogenic effects for mice within 4 weeks of infection was dissimilar between these two strains. These differences can be explained by the difference of immune response between host species and by the difference of immune phase. First, strain 198 could proliferate, but ATCC 25291 was rapidly eliminated in THP-1 cells (Table 3). In mouse macrophages mycobactericidal activity is attributed to nitric oxide produced by inducible nitric oxide synthase [20], whereas in human macrophages, it is attributed to Toll-like receptor signaling-dependent production of anti-microbial peptides [21,22]. Strain 198 is capable of proliferating under these two patterns of mycobactericidal activities, which suggests that strain 198 may have some virulence factors advantageous to survive both in human and mouse macrophages against mycobactericidal activity of the hosts, in contrast to ATCC 25291 which may lack virulence factors to survive in human macrophages. Second, strain 198 showed high bacterial load in lungs continuingly during 16 weeks of infection in mice, while ATCC 25291 proliferated after initial reduction in lungs at 4 weeks of infection (Fig. 1). The *in vitro* infection model using cell lines and the *in vivo* infection model using mice within 4 weeks reflects early stages of infection; on the other hand, the *in vivo* model after 8 weeks reflects chronic phase of infection [17,23]. The difference of pathogenic effects for mice within 4 weeks of infection suggests that strain 198 may resist both innate and acquired immunity, while ATCC 25291 may resist acquired immunity only. We assume that strain 198 and ATCC 25291 may possess different virulence mechanisms to persist in *in vivo* after development of acquired immunity.

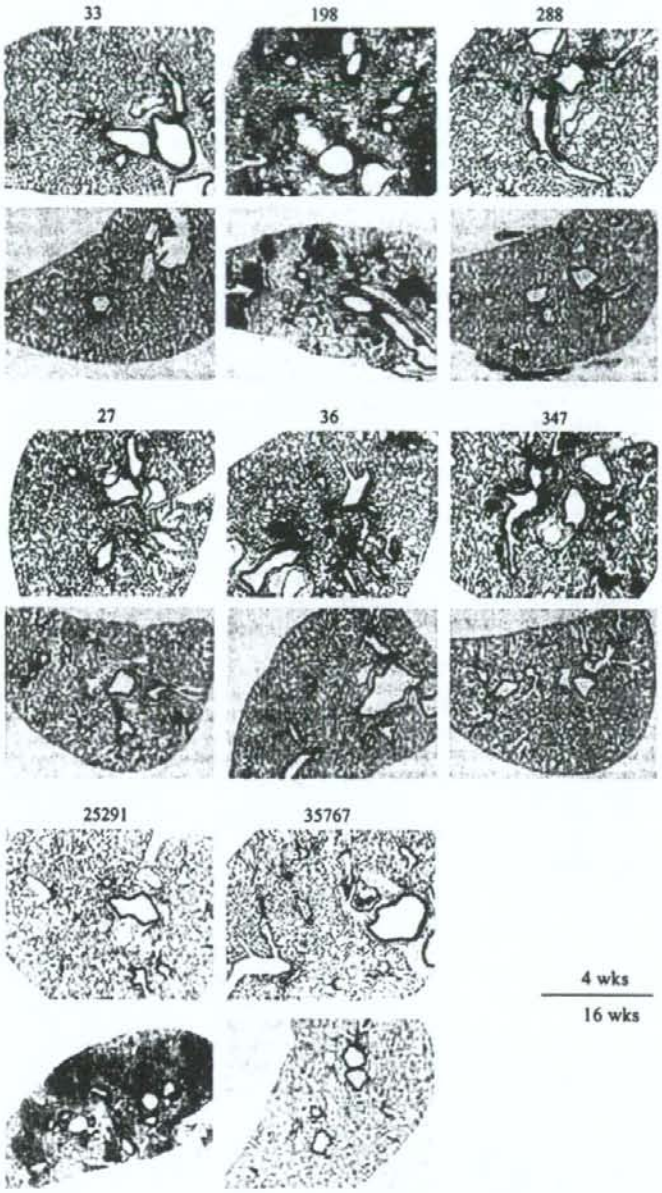

Fig. 2. Histological pictures of the lungs during 4 weeks or 16 weeks of infection in C57BL/6 mice by hematoxylin–eosin staining. Magnification, ×40.

In this study, clinical strains except for strain 198 did not show consistent virulence-associated phenotype among THP-1 cells, C57BL/6 mice, and clinical disease outcome. Similarly, Pedrosa et al. has also revealed that the growth of MAC in bone-marrow derived macrophages does not necessarily predict the virulence in mice by comparing the growth of 41 MAC isolates from various derives including humans, animals, and environment [12]. Although some clinical cases of pulmonary MAC disease may be caused by hypervirulent strains such as strain 198, these findings of clinical and natural isolates suggest that virulence may not the only determinant of the pathogenesis of pulmonary MAC disease in the majority of clinical cases. The development of pulmonary MAC disease depends on the balance between bacterial virulence and host defense. It is widely accepted that patients with pulmonary MAC disease have some characteristics of clinical background, such as males in their 40s and early 50s who have a history of cigarette smoking and excessive alcohol use, and such as postmenopausal, nonsmoking females [3], and these patient characteristics might

possibly indicate unknown predisposing conditions which enhance susceptibility for pulmonary MAC infection. The diverse phenotype of clinical MAC strains may be attributed to the disease susceptibility of the hosts. We propose that pathogenic mechanism of human pulmonary MAC disease include two patterns; one is that the strong virulence of MAC strains such as strain 198 induces rapid mycobacterial growth and serious disease outcome, and the other is that relatively weak to moderate virulence interacts with predisposing conditions of the host, leading the wide range of clinical outcome.

This study was preliminary in that we did not identify the mechanism of hypervirulence of strain 198. We observed the consistency between hypervirulence in human macrophages bedsides in immunocompetent mice and severe clinical outcome only in strain 198, not in any other isolates studied. From this finding, we speculate the existence of strain-specific virulence factors of strain 198. Recent exponential advances have enabled whole genome sequence of two *M. avium* strains, *M. avium* 104 and *M. avium* subsp. *paratuberculosis* K-10. Based on these exhaustive information, comparative genomics of MAC organisms has revealed the different genomic components regarding virulence factors, such as *ser2* encoding glycosylation enzyme of the lipopeptide core to generate the glycopeptidolipids, mammalian cell entry (*mce*) gene homologs, and PE/PPE genes (i.e., with Pro Glu and Pro Pro Glu motifs) [24]. In addition, there are large sequence polymorphisms among MAC organisms, suggesting a large corresponding diversity in virulence [11,24]. We speculate that the virulence of MAC strains including strain 198 may be determined by insertion or deletion of virulence genes encoding known [24] or unknown virulence factors.

In summary, we demonstrated that certain clinical strain derived from patients of the progressive pulmonary MAC disease exhibits strong virulence in human macrophages and in immunocompetent mice. Among clinical isolates, strain 198 is the first isolate hypervirulent to both human macrophages and mice. Our data suggest that strain-to-strain differences in virulence may play a significant role in disease progression in humans. Although Sarmento et al. showed that capability of TNF-α production from macrophages inversely correlates with the virulence of MAC strains [25], we could not find such relationship among the isolates (data not shown). In future studies, we will identify the virulence/pathogenicity-associated factor(s) of strain 198 and survey the frequency of strain variation in immunocompetent patients with pulmonary MAC disease.

4. Materials and methods

4.1. Bacterial strains

We used six clinical isolates from non-AIDS patients with pulmonary MAC disease and two laboratory strains, *M. avium* ATCC 25291 (serovar 2) and *M. avium* ATCC 35767 (serovar 4), in this study. Clinical isolates were obtained between September and November in 2003 at Toneyama National Hospital. Informed consent was obtained from all patients according to the guideline of Institutional Review Board of Toneyama National Hospital. Diagnosis of pulmonary MAC disease was made according to the American Thoracic Society guideline [3]. The samples were derived from two groups of patients; one group exhibited progressive disease in spite of the combination chemotherapy including clarithromycin, ethambutol and rifampin recommended by the American Thoracic Society guideline (progressive type) [3], the other displayed no exacerbation without anti-microbial chemotherapy for approximately ten years or more (silent type). These types were determined by the laboratory findings at the period of sputum sampling (including sputum smear and culture, chest X-ray findings, and erythrocyte sedimentation rate) and the rapidness of disease progression (Table 1). Sputum specimens were mixed with 2% sodium hydroxide, and *N*-acetyl-L-cysteine and then centrifuged for 15 min at 3000 *g*. The supernatants were discarded, and the sediment was mixed at 1:10 (vol/vol) with sterile water. The bacteria were cultivated in Middlebrook 7H9 broth supplemented with albumin–dextrose–catalase, 0.02% glycerin and 0.05% Tween 80, and then kept at −80 °C until following experiments. Identification of MAC was made by polymerase chain reaction using a commercially available kit (AMPLICOR Mycobacterium Tuberculosis Test, Roche, Basel, Switzerland). The serovars of clinical isolates were identified by the liquid chromatography/mass spectrometry as described previously [26]. Strains not containing serovar-specific oligosaccharides were defined as apolar type.

4.2. Growth in 7H9 broth

Bacterial suspension was adjusted to be 0.2 by optical density (OD) at 630 nm. The samples were cultured in 5 ml of 7H9 media in plastic tubes without agitation After vortexing to dissolve aggregates, cultivated bacterial suspensions were inoculated at days 1, 3, and 5 by serial 10-fold dilutions on Middlebrook 7H11 agar plates supplemented with oleic acid–albumin–dextrose–catalase, and 0.05% glycerol (7H11-OADC) agar plates in triplicate. The number of CFUs was counted after cultivating at 37 °C for 3 weeks.

4.3. Infection of THP-1 cells with MAC in vitro

THP-1 cells were purchased from Health Science Research Resources Bank (Tokyo, Japan). The cells were cultured in RPMI1640 containing 10% heat-inactivated fetal bovine serum (FBS; Equitech-bio, TX), and subcultured every 3–4 days. THP-1 cells were differentiated by 100 nM PMA (Sigma–Aldrich, St Louis, MO) for 48 h before infection. Before 48 h of infection, 1 ml of 2×10^5/ml cells was cultured in RPMI1640 containing 5% human serum (AB-blood group) in 24-well plates. Then, 1 ml of 2×10^4 CFUs/ml bacteria was exposed to the cultured cells for 24 h without opsonization (multiplicity of infection; 0.1 bacteria/cell). After that, the cells were treated with 20 μg/ml of gentamicin for 3 h to kill extracellular bacteria, followed by washing 4 times by RPMI1640. The infected cells were cultured in 2 ml of RPMI1640 containing 5% human serum. At days 0 and 7, uninfected bacteria were removed by washing with RPMI1640 4 times, and 500 μl of filter-sterilized phosphate buffered saline containing 0.5% Triton X-100 (Wako, Osaka, Japan) was treated per well to lyse cell membrane. The intracellular survival of bacteria was determined by counting CFUs by inoculating the cell lysate on 7H11-OADC agar plates. The experiment was performed in triplicate.

4.4. Assays for cytotoxicity

Cytotoxic effects were evaluated by the release of LDH from the cells. LDH activity of culture supernatants was determined by a commercially available kit (Roche, Basel, Switzerland). Supernatants were diluted to be 10^{-1} by distilled water for optimal reaction. The diluents were reacted with reaction mixture for 30 min, and then the OD was measured at 492 nm. Supernatants of completely lysed uninfected cells with filter-sterilized phosphate buffered saline containing 20% Triton X-100 and those of uninfected cells untreated with Triton X-100 were served as high and low controls, respectively. Cytotoxicity (%) was calculated as follows; $(OD_{sample} - OD_{low\ control}) \times 100/(OD_{high\ control} - OD_{low\ control})$. The measurement was performed in triplicate.